Supporting Online Material for

Multiple Spectral Inputs Improve Motion Discrimination in the Drosophila *Visual System*

Trevor J. Wardill[1+], Olivier List[1+], Xiaofeng Li[1,2+], Sidhartha Dongre[1], Marie McCulloch[1], Chun-Yuan Ting[3], Cahir J. O'Kane[4], Shiming Tang[2], Chi-Hon Lee[3], Roger C. Hardie[5] and Mikko Juusola[1,2*]

[1]*Department of Biomedical Science, University of Sheffield, Sheffield S10 2TN, UK,* [2]*State Key Laboratory of Cognitive Neuroscience and Learning, Beijing Normal University, Beijing 100875, China,* [3]*Eunice Kennedy Shriver National Institute of Child Health and Human Development, National Institutes of Health, Bethesda, MD 20892-5431, USA,* [4]*Department of Genetics, University of Cambridge, Cambridge CB2 3EH, UK,* [5]*Department of Physiology, Development and Neuroscience, University of Cambridge, Cambridge CB3 2EG, UK*

This file includes:
Materials and Methods,
Questions and Answers Section,
Tables S1 and S2,
Figs. S1-S14,
References

Materials and Methods

Drosophila Genetics

Fly stocks. Drosophila mutants and transgenic stocks were obtained from the following sources; $ninaE^{5,7,8,9,11,13}$ and $ninaE^{17}$ with $rosy^{506}$ and/or $ebony^{sooty}$ stocks from William Pak (Purdue University) and Bloomington Stock Centre; $ninaE^{I17}$ without any other markers, from the *Drosophila* Genetic Resource Center (Kyoto, Japan); $norpA^{36}$ (aka. $norpA^{P24}$), and ort^{5} from Roger Hardie (ort^{5} was then recombined with wild type (Canton-S) to remove the *scarlet* marker); Hdc^{JK910} from Erich Buchner (University of Würzburg). Rhodopsin3 (with peak UV sensitivity) rescue constructs, labeled as *"[Rh1+ Rh3]"* in this paper, were a gift from Charles Zuker (Columbia University). P-element inserts of *[Rh1+Rh3]* on different chromosomes were tested, and all contained a Rhodopsin1 promoter that drove the expression of Rh3 in photoreceptors R1-R6 exclusively (*32*). A P-element rescue for the *norpA* mutants, labeled as "[Rh1+*norpA*]" in this paper, was a gift from Steve Britt (University of Colorado). The [Rh1+*norpA*] rescue used the Rhodopsin1 promoter that drove the expression of *norpA*-cDNA in photoreceptors R1-R6 exclusively (*43*). The UAS-GCaMP3.0 (*44*) was a gift from Vivek Jayaraman (HHMI Janelia Farm), 3A-Gal4 (*45*), which labels vertical system lobula plate cells, was a gift from Martin Heisenberg (University of Würzburg).

Optimization of genotype. Many genetic manipulations have unwanted side effects that can potentially invalidate results (*46*). To minimize such effects, we attempted to find a rhodopsin1 (Rh1 aka. *ninaE*) mutant that was completely non-functional for phototransduction, rather than being a traditional null allele that prevented protein production. It was important that Rh1 was expressed but non-functional for phototransduction because *ninaE* is required for the structural formation of rhabdomeres (*33*, *47*) (**fig. S1**). To confirm if phototransduction and neurotransmission machinery respond similarly to wild type, we rescued various *ninaE* mutants with a *[Rh1+Rh3]* P-element (*32*) and used electroretinograms (ERGs) to validate the response properties of *ninaE* and *[Rh1+Rh3]* rescued *ninaE* mutants (**fig. S2**). To ultimately confirm the response properties, we recorded intracellularly (see intracellular electrophysiology methods below) and also patch-clamped dissociated photoreceptors in controlled conditions to determine their spectral sensitivity (see patch clamp electrophysiology below). Furthermore we checked the structural formation of the rhabdomeres using transmission electron microscopy (**fig. S1**). Such EM-inspection was also performed for flies that expressed calcium-reporters in the lobula plate tangential cells, shown for TN-XXL (**fig. S1G**); here, DB331-Gal4 (*48*) and TN-XXL (*49*) were gifts from Alexander Borst (Max Planck Institute of Neurobiology). We found that expressing calcium-reporters in the lobula plate neurons had no obvious influence on the rhabdomere structure.

In the process of testing *ninaE* mutants for physiological function, we also tested stocks labeled as "$ninaE^{I17}$", from two unnamed *Drosophila* vision labs. By test crossing these stocks to $ebony^{1}$ and $rosy^{506}$, we found that neither *rosy* nor *ebony* mutations were visually present. When these stocks were rescued with *[Rh1+Rh3]*, both were found to lack neurotransmission from R1-R6, based on electroretinogram testing (See **fig. S2**). These stocks are most likely ora^{JK84} or $ninaE^{1}$ with a deletion that covers *ort* and *ninaE*, but this was not confirmed with PCR, however both labs were informed of the stocks mislabeling. It is therefore probable that using these flies, which have non-functional motion pathway (and potentially color pathways as *ort* is used for R7-R8 synapses), for testing specific visual motion behaviors (*9*, *50*) could bias the interpretation of results. We also investigated the spectral sensitivity of $ninaE^{17}$ R1-R6 photoreceptors with whole-cell patch-clamp *ex vivo*. The results confirmed the earlier findings (*51*) that these cells generate weak residual light-induced activity (**fig. S3**, **A** and **B**).

To generate *Drosophila* with effectively non-functional but intact R7/R8 photoreceptors, we combined the $norpA^{36}$ mutant, with a P-element *[Rh1+norpA-cDNA]* rescue. The $norpA^{36}$ mutant is a strong hypomorph, requiring extreme intensities (much brighter than the normal experimental conditions used in this paper) to activate even a residual, slow light response (*52*). Furthermore, $norpA^{36}$ has been shown to have intact R7 photoreceptors, 6 weeks post-eclosion (*53*) and confirmed here (**fig. S1H**). These lines were also used to generate UV-flies with non-functional, but intact R7/R8 photoreceptors.

To minimize background genetic effects, we replaced all chromosomes without P-element insertions, with chromosomes from a single wild-type (Canton-S) stock. To do this most efficiently, we created a temporary triple balancer stock; FM6/FM7; If/CyO; MKRS/TM6b. This stock produced very few offspring and so to obtain sufficient offspring, we intercrossed two stocks (FM6/FM7; If/CyO; + [CantonS]/TM6b and FM6/FM7; If/CyO; + [CantonS]/MKRS).

Fly crosses. UV-flies for testing functionality (phototransduction and synaptic transmission to large monopolar cells, LMCs) by ERG (**fig. S2**) were first generated by combining *P[ry$^+$,Rh1+Rh3]* on the second chromosome with selected *ninaE* and *ort* mutants on the third chromosome using standard fly crossing techniques using the triple balancer stocks described above. Once *ninaE^8* was identified as a suitable genetic background by ERG and EM (**figs. S1-S2**), the P-element *[ry$^+$,Rh1+3]* from a third chromosome stock was added to the *ninaE^8* chromosome by homologous recombination (*P[ry$^+$,Rh1+Rh3],ninaE^8*).

The ninaE^8 mutant (aka. *ninaE^{P334}*) contains three missense mutations within the sixth transmembrane domain: Thr(283)Met, Trp(289)Arg and Cys(297)Ser (*54*). *ninaE^8* produces 0.0004% of wild-type rhodopsin levels, which substantially slows the degradation of rhabdomeres when compared with the null mutant, *ninaE^{17}* (*54*). In dissociated cells, the residual sensitivity to visible light of both *ninaE^8* flies (**Fig. 3G**) and the UV-flies derived from this stock (**Fig. 1C**) was ~10^6 fold reduced compared to wild-type in the range 500-560 nm and undetectable beyond 560 nm, and could not therefore plausibly contribute to physiological or behavioral responses measured *in vivo*. Furthermore, across the tested spectral range *ninaE^8* R1-R6s were about 10-fold less light-sensitive than those of the supposedly null mutant *ninaE^{17}* (**fig. S3B**). The identity of the opsin responsible for the residual sensitivity in *ninaE^{17}*, which has been reported previously (*51*), is unknown.

Flies lacking functional R7/R8 were generated either by crossing wild-type flies bearing a P element containing *norpA* cDNA under a Rh1 promoter (P*[Rh1+norpA])* with a *norpA^{36}* mutant, or by performing similar Rh3 rescue. As a further control for the Rh1-rescue, such flies from another stock (a gift from Thomas R. Clandinin, Stanford University, CA) were tested in the flight simulator (details below); their optomotor responses resembled those of our own flies. UV-flies lacking functional R7/R8 were generated by recombining P*[Rh1+norpA]* onto the UV-fly third chromosome by homologous recombination and then using this chromosome to rescue the *norpA^{36}* mutant. The obtained line (*w$^+$,norpA^{36};P[w$^+$,Rh1+norpA],P[ry$^+$,Rh1+3],ninaE^8*) did not show any R7/R8 response to amber or green stimuli equivalent to genotype 28 in **figure S2**.

Generation of transgenic Rhodopsin-specific norpA rescue flies. norpA cDNA fragment was purified from 5'-NotI to 3'-XbaI, digested pcDNA3-*norpA* construct (gift from Craig Montell, Johns Hopkins University) and used to replace the Gal4DBD fragment of X11-pCaST-Gal4DBD (*55*) with the same restriction sites. The resulting construct, pCaST -*norpA*, was used as a template for the following subcloning procedures:

The Rh3 (-526 to +19; 545 bps) and Rh4 (-1541 to +552; 2093 bps) promoter fragments were PCR-amplified from genomic DNA of wild-type (Canton S) flies and inserted into pCaST -*norpA* (via the Pme I site) to generate pCaST -Rh3-*norpA* and pCaST -Rh4-*norpA* constructs by standard DNA ligation method. The Rh5 (-3762 to +73; 3835 bps) and Rh6 (-1593 to +138; 1731 bps) promoter fragments were PCR-amplified and inserted into pCaST -*norpA* (at the Not I site) to generate pCaST -Rh5-*norpA* and pCaST -Rh6-*norpA* using the In-Fusion cloning system (Clontech). The resulting constructs contain *norpA* cDNA under the control of rhodopsin promoters. The constructs were validated by DNA sequencing. The PCR primers are as follows:

Rh3 promoter:

Forward: 5'-GCAGCTGACTGCACTGAATTTTGTAG-3'

Reverse: 5'- GGTCTGCGGGCCAAGACGA-3'

Rh4 promoter:

Forward: 5'-ATGATATCTCGCGTGTCATCCAGAACTTTG-3'

Reverse: 5'-ATGTTTAAACCGGTCAACCCGATACCGAAC-3'

Rh5 promoter:

Forward: 5'- TGTTTAAACGCGGCCGCGTGCCCGTCATTTTGCTTAT-3',

Reverse: 5'-GATCTCGAGGCGGCCGCACTGCTTGATCCGCTCCAAA-3'

Rh6 promoter:

Forward: 5'-TGTTTAAACGCGGCCGCACATGTTGCCTCATTGAATCAG-3'

Reverse: 5'-GATCTCGAGGCGGCCGCTTCGAATGGCTGGTACTGGT-3'.

Transgenic flies were generated by standard P-element-mediated transformation. For each construct, 3-5 independent insertions were crossed into the *norpA* mutant background and transgene-mediated *norpA* expression in the eyes was examined by anti-norpA staining. The transgenic lines that express *norpA* only in the desired photoreceptor subclasses were selected for subsequent analyses.

UV-flies with calcium indicators were made by introducing the P-element *[w^+,Gal4-3A]* to our UV fly third chromosome by homologous recombination and then adding this chromosome to a fly with P*[y^+,UAS-GCaMP3.0]* using standard fly crossing procedures (P*[y^+,UAS-GCaMP3.0]; P[ry^+,Rh1+Rh3], ninaE*^{8}).

ERGs. Flies were mounted inside a copper cone and their temperature controlled by a peltier element (*12*) to 25°C. To test the spectral sensitivity, three wavelengths were chosen for stimulation. Before each stimulus, flies were dark adapted for 3 minutes. The reference electrode was placed in an ocellus, while a blunt recording electrode was placed on the stimulated eye. Both electrodes were borosilicate glass, filled with fly Ringer (containing in mM: 120 NaCl, 5 KCl, 10 TES, 1.5 $CaCl_2$, 4 $MgCl_2$, and 30 sucrose (*12*)). The software and electrophysiology setup were as previously reported (*56*). All flies tested were female with a homozygous w^+ (red eyed) background (except the *[Rh1+norpA]* stock, which was heterozygous w^+/w^{1118}) and 5 days post-eclosion.

ERG light stimulus. To ensure a uniform and reproducible stimulation of the eye, we used high-power light-emitting diodes (LEDs) as a light source, which were interchangeable and mounted on a cardan arm system. To obtain saturating responses from photoreceptors R1-R8 we chose UV (full-width 385 ± 30 nm; 390 mW), Cyan (full-width 505 ± 35 nm; 130 mW) and Amber (full-width 590 ± 40 nm; 75 mW) LEDs. All spectral widths were measured with a spectrometer (1 nm typical resolution) to verify their manufacturer's specifications and the Cyan LED had a 535 ± 35 nm bandpass filter mounted before the lens to further reduce short wavelengths, so as not to excite Rh3 pigments. Each LED, when mounted in position, was projected by a 25 mm lens onto the centre of the eye (~20 mm from lens; subtended angle 48 ± 2°) and driven by an OptoLED using the optical feedback option to accurately maintain light levels during and across experiments. The stimulus was composed of 700 ms of darkness, 700 ms of light, followed by 700 ms of darkness. This cycle was flashed 10 times in consecutive square-wave pulses. In some rare cases, responses were briefly contaminated with spurious electrical noise, and so additional consecutive stimuli were added, up to 15 in total, so as to obtain the first 10 noise-free recordings. The saturating peak responses, evoked by the stimulus, were not compromised by a prolonged depolarizing after-potential, as previously confirmed by intracellular recordings in wild-type photoreceptors (see Fig S1C in (*46*)).

ERG analysis. The influence of fast light adaptation meant that all flies kept in darkness for 3 min displayed responses in traces 1–4 significantly different from each other and from the rest of the recorded traces as previously confirmed by intracellular recordings in wild-type photoreceptors (see Fig S1C in (*46*)). Therefore, only traces 5–10 were used to obtain a representative Figure for each fly or condition. For each fly strain, the first 5 (n) flies that produced reliable data from all traces are reported in this paper, out of a total of 10 flies tested. For each genotype and wavelength, the mean and SEM were calculated however the SEM was omitted for clarity. The data acquisition and stimulus protocols were executed under Matlab using custom-written software (Biosyst (*12*, *37*)) with an interface package for National Instruments boards (MATDAQ; H. P. C. Robinson, 1997–2007). Origin software was used for the data analysis and plotting.

Transmission Electron Microscopy. The dissection, fixation embedding, sectioning and imaging protocols for EM were as previously described (*30*, *38*, *57*). To summarize, fly heads were dissected under a drop of 2.5% glutaraldehyde, 2.5% paraformaldehyde in 0.1 M sodium cacodylate/HCL buffer (pH 7.3) and then fixed in the same solution for 2 h at room temperature. After washing in cacodylate buffer, the samples were placed in 1% osmium tetroxide in veronal acetate for 2 h at 4 °C. After further washing, the samples were dehydrated for 7 min in alcohol in each of the following concentrations: 50%, 70%, 80%, 90%, 95%, and 100%. The dehydration with 100% ethanol was repeated two times. For the last change, the ethanol used had been dried over anhydrous copper sulfate. Next, the samples were placed in two 10-min changes of propylene oxide (PPO). For embedding, the specimens were placed in a 50/50 mix of PPO and Epon resin overnight. The next day, the specimens were put into several changes of fresh resin and placed in an oven at 60 °C for 12 h. Serial 60-nm sections were stained with uranyl acetate and lead citrate and examined at 80 kV in an electron microscope. Images were captured with a cooled MultiScan wide-angle CCD camera (sidemounted; 1,024 × 1,024 pixels).

Intracellular electrophysiology

Flies. UV-flies (with and without functional R7/R8 photoreceptors), *ninaE*^{8} mutants, rhodopsin-specific *norpA* rescue transgenic flies and WT Canton-S strains were used in electrophysiological recordings. We also tested electrophysiological functions of photoreceptors and LMCs in transgenic flies that expressed calcium-reporters in their lobula plate tangential cells (LPTCs), having either UV- or WT eye phenotypes, and found that their response properties (temporal dynamics and spectral sensitivity) unchanged. Therefore, **Figure 2** shows pooled R1-R6 photoreceptor and LMC results from UV-flies with or without LPTCs' calcium-reporters. Flies were reared on standard medium at 18°C in 12:12 light:dark cycle and females were selected for electrophysiological experiments 3-10 days after eclosion.

Preparation. Flies were immobilized inside a tight metal tube of a conical fly holder and that their protruding heads were fixed in a preferred position with beeswax, as previously described (*12*, *13*, *58*). To allow the recording microelectrode to enter the retina/lamina, a small hole, size of few ommatidia, was cut in the dorsal cornea and sealed with Vaseline to prevent the eye from drying.

In vivo recordings. Intracellular voltage responses were recorded through sharp quartz or borosilicate microelectrodes, having 120–250 MΩ resistance. Recordings from R1-R6 photoreceptors and large monopolar cells (LMCs) were performed separately, using 3 M

KCl intra-electrode solution (photoreceptors) and 3 M potassium acetate with 0.5 mM KCl (LMC; to minimize reduction in the chloride battery). A blunt reference electrode was inserted into the fly head capsule close to the ocelli. The head temperature of the flies was kept at 21 ± 1°C, unless stated otherwise, by a feedback-controlled Peltier device. The recordings were mostly performed after 2-5 minutes of dark adaptation using the discontinuous (switched) clamp method (*59*, *60*) with a switching frequency of up to 50 kHz. The capacitance of the electrodes was compensated by monitoring the head stage output voltage. Stimulus generation and data acquisition were performed by Biosyst (*12*, *37*). The stimuli and responses were typically sampled at 1-10 kHz, low-pass filtered at 500 Hz (low pass dual channel elliptic filter or custom-built Bessel filters with steep cut-off) and stored in the hard drive for off-line analysis.

Light sources. The light stimulation was transmitted through a randomized quartz fiber optic bundle (spectral transmission range: 180-1,200 nm) either from chosen LEDs (the same as for ERG recordings, above; UV-LED, full-width: 390 ± 40 nm or LXHL-PR03 Royal Blue, full-width: 455 ± 30 nm, 220 mW) or from a customized monochromator system (details below), secured on a Cardan arm system. This arrangement enabled free positioning of the light source with equal distance to the eye with the light output subtending <5°, as seen by the fly. Thus, spatially, the stimuli fitted well inside the typical receptive field of a R1-R6 photoreceptor (*38*). After locking the light source at center of the receptive field, voltage responses of the cells to chosen color stimuli were measured from the same point in space. The responsiveness of the cells was tested by repeated presentations of light pulses or by naturalistic light intensity series (10,000 points/s). Naturalistic contrast, c, stimulus patterns ($c = \Delta I/I$) were selected from the van Hateren natural-stimulus-collection (*61*); ΔI = change in intensity, I. The spectral outputs of all the light sources were measured and calibrated by using spectrometer (250 to 1,000 nm). The spectrometer recordings confirmed the maximum light level wavelength distribution of the LEDs (which was surprisingly narrow); we normally used them below this level, so any potential error in our spectrometer sensitivity would be avoided in each experiment. *In vitro* patch-clamp results demonstrated that the spectral sensitivity of R1-R6 photoreceptors from UV-flies to long-wavelength light (>500 nm) was 10^5-10^6 times less than their UV-sensitivity (**Fig. 1C**). Furthermore, for amber stimuli, both UV-flies and *ninaE*^{8} mutants were at least 10^6-times less sensitive than wild-type R1-R6s (**Fig. 3G**). Therefore, use of additional bandpass-filters was not warranted.

Selection criteria. Electrophysiological identification of R1–R6 photoreceptors and LMCs is straightforward as the former depolarize (*12*) and the latter hyperpolarize (*51*, *58*, *62*) to given spectrally white light pulses with characteristic response waveforms. Both in the UV- and WT-flies, their response waveforms are very similar at the lamina input level (**fig. S4**, **A** and **B**), while the differences in responses between different LMC subtypes can be subtle (*13*, *58*). In *Calliphora* lamina, L1 and L2 generate similar voltage responses, while more hyperpolarized L3 show augmented off-transients (*63*). In *Drosophila*, LMC subtypes have not been electrophysiologically identified, but as L1 and L2 are the largest lamina interneurons most recordings were probably in them. It is also possible that some responses were from L3 or from processes of amacrine cells that share histaminergic input with L2 and L1 cells (*51*). Nonetheless, it is our experience so far that fast hyperpolarizing responses to light pulses in *Drosophila* lamina (*13*, *58*), given at the centre of a LMC's receptive fields, display rather similar characteristics (**Fig. 2**, **A** and **B**). The small dimensions of L4 and L5 monopolar cells (*64*) and their non-histaminergic inputs (*65*), makes it unlikely that any recordings would be from them.

Only stable high quality recordings were used. For WT and UV-flies, the selected R1-R6 photoreceptors had typically resting potentials ≤−60 mV in darkness, where their maximum impulse responses were ≥40 mV (**fig. S1C**). For the selected LMCs, their resting potentials were ≤−30 mV and maximum responses ≥15 mV. For the chosen data, we found that the larger responses displayed similar general dynamics to the smaller responses. For *ninaE*^{8} mutants, the pre- and postsynaptic responses were significantly smaller (typically ≤5 mV), but had similar amplitudes, sensitivity and stability to the responses of UV-flies to green-yellow light pulses, indicating that their inputs came from R7/R8 photoreceptors. Note that because *ninaE*^{8}-LMCs only receive indirect R7/R8 inputs, finding their narrow receptive fields was particularly difficult. Thus, stable responses of seven LMCs and seven R1-R6 axons with R7y(Rh4) + R8y(Rh6) sensitivity; two LMCs and two R1-R6 axons with R7p(Rh3) + R8p(Rh5) sensitivity and two R1-R6 axons with R7(Rh4) sensitivity were ever recorded *in vivo* in nine *ninaE*^{8}-flies after considerable efforts (**Fig. 3**, **H** and **I**; **fig. S5**, **C** and **D**).

We did not use dye-injections to directly determine, which R1-R6 photoreceptors received R7/R8 inputs. This is because:

(i) obtaining high-quality intracellular recordings with high-impedance sharp microelectrodes from very small *Drosophila* photoreceptors is by itself challenging. To detect the relatively weak R7/R8 inputs, the electrode needs to be inserted close to the gap junction. This preferably requires impaling the axon, which is very narrow (≤1 μm), and necessitates the impaling electrode tip to be very sharp (approx 50 nm).

(ii) filling photoreceptors electrophoretically with the same electrode is even harder; dyes increase the electrode impedance further, thereby increasing the recording noise, reducing the useful signal range, making compensation unreliable and blocking the electrode tip frequently. Larger electrode tips could be used for filling cells, but these are not likely to be able to impale the fine axons near the gap junctions and so it would not be possible to identify their relative spectral voltage changes.

Intracellular membrane properties. To verify that the integrity of the photoreceptor membrane was not significantly affected by genetic interventions, we examined its electrophysiological properties. This was done by current pulse injections in current-clamp mode after compensating the capacitance of the recording microelectrode, as in (*12*, *60*). Current pulse was injected via the recording electrode and the resulting voltage output was typically averaged over 10 repetitions (**fig. S4**, **C** and **D**; **fig. S6**, **B** to **E**).

To establish that R1-R6 photoreceptors and LMCs of UV-flies (sensitive only to <450 nm stimuli) receive inputs from R8 directly through functional contacts (and not indirectly through extracellular field), their membrane potential was lowered in darkness by hyperpolarizing current pulse. For example, below -70 mV, voltage-sensitive K+-channels in photoreceptor membrane close, linearizing its membrane's current/voltage relationship (*66*). A long-wavelength flash (545 or 595 nm; invisible to UV-sensitive R1-R6 photoreceptors, **Fig. 1C**) was then given to stimulate the R8 photoreceptor, which collects light from the same point in space as the tested R1-R6. Finally, the change in resistance, as a signature of direct increase in input conductance, was obtained by subtracting the light- and current-induced responses from their combined response and by dividing this difference with the current step in darkness (**fig. S6**, **B** to **E**).

Signaling performance estimates. Signal and noise components of photoreceptor voltage responses were estimated as in (*12*, *37*, *38*). The signal was obtained from the average of consecutive 1,000 ms long voltage responses to a repeated naturalistic light intensity pattern, and its power spectrum was calculated using Matlab's Fast Fourier Transform (FFT) algorithm. Only steady-state adapted responses were analyzed; first 10-20 responses were omitted because of their adaptive trends. The noise was the difference between individual responses and the signal, and its power spectra were calculated from the corresponding traces (*67*). Therefore, for an experiment using *n* trials (with *n* = 50–110), there was one signal trace and n noise traces. Both signal and noise data chunks were divided into 50% overlapping stretches and windowed with a Blackman-Harris-term window, each giving three 500-point-long samples. Thus, we obtained 150–330 spectral samples for the noise and three spectral samples for the signal. These were averaged, respectively, to improve the estimates.

A triple extrapolation method (*37*) was used to estimate the rate of information transfer, *R,* of steady-state-adapted photoreceptor voltage responses to naturalistic stimulus, NS. This method, unlike SNR analysis, requires no assumptions about the signal and noise distributions or their additivity.

Photoreceptor voltage responses were digitized by sectioning them into time intervals, *T*, that were subdivided into smaller intervals *t* = 1 ms. (Only dim luminance data was down-sampled to 125 Hz, giving *t* = 8 ms, which better represented their slow dynamics). This approach captures 'words' of length *T* with *T*/*t* 'letters'. The mutual information between the response, *s*, and the stimulus is then the difference between the total entropy:

$$H_S = -\sum_i P_S(s_i)\log_2 P_S(s_i) \tag{1}$$

and the noise entropy:

$$H_N = -\left\langle \sum_{i=1} P_i(\tau)\log_2 P_i(\tau) \right\rangle_\tau \tag{2}$$

where $P_i(\tau)$ is the probability of finding the *i*-th word at a time *t* from the onset of the trial. This probability $P_i(\tau)$ was calculated across trials to the repeated NS. The values of the digitized entropies depend on the length of the 'words' *T*, the number of voltage levels *v* and the *size* of the data file, $H^{T,n,size}$.

The estimates for the entropy rate, R_S, and noise entropy rate, R_N, were then extrapolated from the values of the experimentally obtained entropies to their successive limits, as in (*38*).

$$R = R_S - R_N = \lim_{T\to\infty}\frac{1}{T}\lim_{v\to\infty}\lim_{size\to\infty}\left(H_S^{T,v,size} - H_N^{T,v,size}\right) \tag{3}$$

The rate of information transfer is the difference between the entropy and noise entropy rates (*37*, *68*).

Whole-cell patch-clamp recordings

For whole-cell photoreceptor recordings, dissociated ommatidia were prepared as previously described (*69*) from newly eclosed adult flies and transferred to the bottom of

a recording chamber on an inverted Nikon Diaphot microscope. The bath contained (in mM): 120 NaCl, 5 KCl, 10 *N*-Tris-(hydroxymethyl)-methyl-2-amino-ethanesulphonic acid, 4 $MgCl_2$, 1.5 $CaCl_2$, 25 proline and 5 alanine, pH7.15. The intracellular pipette solution was (in mM): 140 K gluconate, 10 *N*-Tris-(hydroxymethyl)-methyl-2-amino-ethanesulphonic acid 4 Mg-ATP, 2 $MgCl_2$, 1 NAD and 0.4 Sodium-GTP, pH 7.15. Whole-cell voltage clamp recordings were made at room temperature (20 ± 1° C) at –70 mV (including correction for –10 mV junction potential) using electrodes of resistance ~10-15 MΩ. Series resistance values were generally below 30 MΩ and were routinely compensated to >80%. Data were collected and analyzed using an Axopatch 200 amplifier and pCLAMP10 software.

Measuring spectral sensitivity

Ex vivo dissociated ommatidia. To quantify any residual long wavelength sensitivity of UV-fly photoreceptors expressing Rh3, we used monochromatic light from a 75W Xe arc passed through a monochromator (Photon Technology Instruments) and delivered by a liquid light-guide via the microscope's front port. At wavelengths longer than 480 nm long pass filters (GG475 Schott or FL0500 Thorlabs) were inserted to eliminate any stray short wavelength light. To accommodate the large (~10^3–10^4 fold) variation of sensitivity across the measured range (400-600 nm), effective intensity was varied by adjusting the duration of the light pulse (2-500 ms) and responses were quantified from the integral light-induced currents (which remained within the linear range). Before calculating relative spectral sensitivity data were corrected for quantal content at different wavelengths, calibrated using a spectrometer. Because the combined optical path transmitted little light in the ultraviolet, measurements were not performed at wavelengths shorter than 400 nm, where the relative spectral sensitivity is estimated to be 0.7% that at peak wavelength (340 nm) using pigment nomograms (*70*), or ~1.3% using measurements of R7p photoreceptors in larger flies (*71*). Cells were also tested using ultra-bright green (570 nm) or amber (590 nm), light-emitting-diodes which delivered maximum intensities equivalent to ~10^7 photons per photoreceptor s^{-1} with respect to wild-type (Rh1 expressing) photoreceptors (calibrated by counting quantum bumps at low light levels).

Similar measurements on *ninaE*^{8} and *ninaE*^{17} R1-R6s established that *ninaE*^{8} is a functional Rh1-null (or near null) mutant as *ninaE*^{8} R1-R6s were about 10-fold less light-sensitive across the tested spectral range than those of the *ninaE*^{17} Rh1-null mutant (**fig. S3B**). Prolonged bright monochromatic stimulation evoked maximally 1-2 bumps/s over the wavelength range of 400-520 nm; in fact, the responsiveness was too low to generate a reliable spectral sensitivity curve (**fig. S3B**). Based on these measurements, we estimate that over the wavelength range (400-520 nm), the sensitivity of *ninaE*^{8} R1-R6s is at least 10^6-10^7-times less than that of wild-type flies, with no detectable responses to monochromatic stimuli of wavelengths longer than 560 nm (**Fig. 1C** and **fig. S3B**). Accordingly, even the maximally bright LED amber pulses (590 nm; see above) rarely evoked single-photon responses (two shown in **Fig. 3G**). Thus *in vivo*, the macroscopic voltage responses of R1-R6 axons and LMCs cannot be caused by residual Rh1-pigment expression, but must be channeled from R7/R8 photoreceptors (**Fig. 3**, **H** and **I**). Although the spectral sensitivity deviates from the 340 nm nomogram, to our knowledge neither absorbance nor sensitivity of any UV pigments have previously been measured with this resolution at longer wavelengths, Consequently, whether the response between 400 and 520 derives exclusively from Rh3, or also includes residual Rh1-pigment or misexpression of a short wavelength rhodopsin such as Rh5 is not clear.

In vivo (intact flies). To measure the intracellular responsiveness of R1-R6 photoreceptors and LMCs to monochromatic stimuli, we used a custom-designed programmable Optoscan monochromator, which supported wavelengths from 300–700 nm and bandwidths from 0–30 nm (the lamp had spectral output range: 250-1,200 nm). Both the center-wavelength and bandwidth could be computer controlled in Matlab, using Biosyst (*12*, *37*) with millisecond time resolution. Because monochromators typically produce residual harmonics (multiples of the peak wavelength) that can be large enough to stimulate photoreceptors, which operate on logarithmic sensitivity scale (for example, 620 nm output comes with a smaller 310 nm harmonic), the light output of the monochomator system for wavelengths longer than 420 nm was filtered by a steep long-pass edge-filter (LP420 nm, having $<10^{-6}$ throughput <420 nm and 99% throughput 420-640 nm). This arrangement removed major harmonics and minimized spectral irregularities of the narrow-bandwidth color pulses, which we used for testing the spectral sensitivity range of photoreceptors and LMCs. The monochromator system's light output (measured from the end of the quartz light guide, facing the fly eye) was calibrated by using a spectrometer. The energy of each narrow-bandwidth color pulse (2-5 nm ± center-wavelength) was measured in 1 nm resolution and equalized by changing the software commands for specific driver settings (input slit, output slit, bandwidth) until its energy integral matched the integrals of all the other pulse energies used. The spectral output of the calibrated monochromator system was retested regularly and found to consistently produce the same range of isoluminant colors, even after lamp changes.

In order to determine responsiveness of R1-R6 photoreceptors and LMCs to monochromatic light, short (10 ms) sub-saturating flashes of 16 wavelengths (± 5 nm) covering 300-620 nm spectral range with 20 nm intervals, were presented to briefly dark-adapted cells at the centre of their receptive fields. To minimize light-induced changes in photoreceptors' rhodopsin/metarhodopsin ratio, the tested cells were typically adapted 2 minutes with 590 nm light before a brief dark-adaptation (1-2 min). As metarhodopsin isomerizes back to rhodopsin by red-light, this method aims to reset the rhodopsin/metarhodopsin equilibrium. In the experiments, we typically used 1-5 s flash intervals (but also sometimes shorter: 0.25-0.5 s to increase traces for averaging) with each monochromatic flash being repeated 10-1,000 times to reduce neural noise; making the full scan of the cell's spectral responsiveness from several to tens of minutes. Therefore, only the spectral responsiveness of long-lasting stable recordings were analysed in this paper.

The voltage responses of *ninaE*^{8} R1-R6 photoreceptors and LMCs are very difficult to record *in vivo*. Their responses are small and finding of their receptive field centres requires very intense light stimuli. Although we made many attempts, we failed to obtain recordings with the monochomator system. The voltage responses shown in **Figure 3** (**H** and **I**) and **fig. S5C** were evoked by four ultra-bright LEDs (see *light sources* in page 5). In the experiments, each cell was sequentially tested in a rapid succession by repeating (typically 10 times) very bright amber, green, blue and UV pulses of comparable energy (as quantified by a spectrometer). The spectral responsiveness of most *ninaE*^{8} R1-R6 photoreceptor axons and LMCs followed the summed spectral sensitivity-functions (nomograms) of R7y/R8y- and R7p/R8p-pairs (**Fig. 3I**). The significance that the responses of the cells in one group (R7y/R8y-sensitivity) differed from those of the other (R7p/R8p-sensitivity) was computed for each tested spectral pulse: 385 nm, p = 0.065; 455 nm, p = 0.001; 505 nm, 0.480; 595 nm, p = 0.010 (one-tail ANOVA Bonferroni-test);

horizontal error-bars show 95% of the absolute bandwidth range of each LED (**Fig. 3I**). Hence, the cells in one group can be reliably distinguished from those in the other by their responses to few spectral pulses. This also makes it impossible for the two different spectral sensitivity profiles of *ninaE*^{8} R1-R6 photoreceptor axons and LMCs to result from a single residual Rh1-pigment expression. Instead, their sensitivity must be unique for their lamina cartridge, as channeled from its specific R7/R8 pair.

In vivo data in **Figures 2D, 2H** and **3I** are given as spectral responsiveness instead of sensitivity, because recording time did not permit testing of the principle of univariance (*72*), which is a necessary assumption to calculate spectral sensitivity and is unlikely to be upheld in a system where parallel chromatic inputs are integrated via gap junctions and/or synapses:

$$\text{Spectral responsiveness } \% = 100 * (V_n/V_{\text{max across spectrum}}) \quad (4)$$

Nonetheless, for **Figure 4H**, we were able to record voltage responses from few stable WT R1-R6s and LMCs to the full set of equal energy spectral pulses and to broad-band LED pulses, which covered 4-log light intensity range. Hence, we could map the spectral responsiveness of these cells into sensitivity by their corresponding V/logI-functions; see for example (*38*). In general, we prefer to show *in vivo* data as recorded or as spectral responsiveness, as these signals represent somewhat undistorted snapshots of the ongoing neural computations. Conversely, sensitivity measures are never fully under control; time- and intensity dependent light-adaptation make the light-history of each recording unique and logarithmic intensity mapping is prone to estimation errors.

Immunohistochemistry

Retinas were dissected from 2-3 days old adult flies and fixed with 4% paraformaldehyde in 0.1M phosphate buffer (pH 7.4) at room temperature for 30 minutes. After three 5 minutes washes with PBT (0.5 % TritonX-100 in phosphate buffered saline), the retinas were blocked with 10% goat serum in PBT and incubated with primary antibodies overnight and followed by three times of washes and overnight incubation of secondary antibodies. The concentrations of primary antibodies were listed as follows: rabbit anti-*norpA* (a gift from Craig Montell), 1:300 dilution; mouse anti-Rh3 (2B1, a gift from Steven Britt), 1:100 dilution. The secondary antibodies including Alexa 488, or Alexa 647 goat anti-rabbit or anti-mouse IgG (Invitrogen) were used at 1:400. The retinas were imaged using a confocal microscope. Image stacks were deconvolved using the Huygens Professional deconvolution Software and rendered using the Imaris software.

Optomotor behavior in *Drosophila* flight simulator system

A tethered fly was connected to the classic torque-meter (*73*, *74*) by a small clamp holding the copper-wire harness, which fixed the fly's head in a rigid position and orientation, but allowed stationary flight (*20*, *75*).

A custom-built, computer controlled flight simulator system was used to study *Drosophila*'s optomotor behavior. A fly, tethered from the torque meter, was lowered by a mechanical manipulator in the center of a black plastic cylinder, which had uniform vertical openings in regular intervals, generating a continuous stripe pattern scene around the fly's long axis. Outside, the cylinder faced 360^{o} white panorama, illuminable

either by a surrounding ring-shaped light-tube (special black light: full-band: 350-900 nm) or from above by LED light (narrow-band) projections; thus, its spectral reflectance could be controlled by either changing colored gelatin filters (diffuse, amber, blue or green; in front of the ring light) or by using LEDs with different spectral outputs (the same LEDs as for ERG and intracellular recordings, above, with additional ultra-bright UV-LED, 365 nm; full range: 350-405 nm). Spectral ranges for these different modes of illumination were measured and calibrated using a spectrometer (see above). Regardless of the light source, the diffuse (and often reflected) motion stimulation was always significantly dimmer (0.5-1.5 log-intensity units) than the direct stimuli used in the intracellular recordings. In the experiments, a flying fly saw a continuous (360^{o}) stripe-scene of predetermined spectral content, which was free of motion artifacts, flashing or aliasing. After one second of viewing the still scene (of preselected spectral content), it was spun to the right by a linear stepping motor for two seconds, stopped for two seconds, before rotating to left for two seconds, and stopped again for a second. This eight-second stimulus was repeated 10 times and each trial, together with the fly's coincident yaw torque responses, was sampled at 1 kHz and stored in a PC's hard-drive for later analysis, using Biosyst (*12*, *37*). Presumably to stabilize gaze, flies tend to follow the scene rotations, generating yaw torque responses (optomotor responses to right and left), the strength of which is believed to reflect the strength of their motion perception (*9*). Stimulus parameters for moving stripe scenes, as shown in the figures, were: azimuth ±360°; elevation ±45°; wavelength, 14°; velocity, 45°/s; contrast, 1.0, as seen by the fly. **Figure 4** and **figure S9** (**A** and **B**) show the averages (*n* = 5-10 flies) of the mean optomotor responses (*n* = 10 trials for each fly) for each tested fly population.

We tested optomotor responses of different flies to moving stripe-scenes of three different spectral contents: black-and-white (full-width: 380-900 nm), black-and-blue (full-width: 430-490 nm) and black-and-amber (full-width: 560-620 nm) as shown in **Figure 4**. To verify that calcium-reporter expression in the lobula plate tangential vs-cells was not degrading optomotor responses, we compared optomotor responses of UV-files with GCaMP3.0 or Cam2 vs-cell expression to those of UV-flies without such expression. UV-flies with calcium-reporters showed normal-like responses (**fig. S9B** and **fig. S11D**). To verify that air flow was not affecting optomotor responses, a transparent cup was placed inside the black plastic cylinder and the field rotation experiments were repeated using the same flies, for majority of the fly strains. Air flow had no effect on the responses (**fig. S9**, **A** and **B**). To verify that ocelli were not significantly contributing to the optomotor responses, some experiments were performed using the same flies before and after their ocelli were covered with thick black paint. We concluded that ocelli had no clear influence on the responses (**fig. S9C**).

Quantifying optomotor behavior. In the flight simulator system, the optomotor responses of individual flies to the same repeated field rotations vary in strength and repeatability (**fig. S10**), but the visual performance of different genotypes is clearly different. These differences can be quantified by measuring the mean torque response of a single fly to 10 stimulus repetitions and by averaging the mean responses of the many flies of the same genotype (typically 10). This cancels out noise and nonsystematic (arbitrary) trends of single experiments, revealing the underlying response strength and characteristics of optomotor behavior for each genotype. These population responses are shown in **Figure 4** for straightforward comparison.

In open-loop experiments, a *Drosophila*'s torque response returns gradually to baseline after the optomotor stimulus stops, but this can take many seconds (varying with

individual flies; *e.g.* (*76*), page 45). Accordingly, in our experiments, which contain only brief 2 second-long inter-stimulus-intervals, the torque responses typically show a small dip (5-10%) during these still periods toward the baseline. Therefore, for comparing the optomotor behavior of different genotypes, we used the maximum range (or peak-to-peak) of the torque response, evoked by the combined leftward and rightward field rotation stimulus. The maximum range and variability in the torque responses to the same optomotor stimulus are shown in **figure S11** with controls (*e.g.* spontaneous activity).

To quantify how reliably individual torque responses to ten-times repeated stimulation differed from the background activity, the mean of 1,000 points before the optomotor stimulus was compared to the mean 1,000 points during the stimulus. Thus, these two groups of means (n = 10) were used to calculate whether the recorded torque responses differed from change level ($p \leq 0.05$; one-tail ANOVA) over the period of each experiment. The number of flies in each genotype that generated significant optomotor responses to every stimulus repetition is summarized in **table S2** for black-white and black-amber stripe field rotations. Although the optomotor behavior of individual flies in each tested genotype contained additional spontaneous activity (*e.g*. **figs S9-S10**), there were at least one fly in each genotype, including those of R7 or R8 *norpA*^{36}-rescues (**Figs. 4D-E**), that showed significant torque responses in each trial to the spectrally broad black-white field rotations. Furthermore, 20-40% of UV-flies/*ninaE*^{8}-mutants showed consistent trial-to-trial responsiveness to the black-amber field rotations (*cf*. **fig. S10**, **A** and **B**). But most importantly, the average torque responses of single flies to ten stimulus presentations (**fig. S10**, thick lines) differed clearly (and thus could be readily distinguished by eye) from the no-responses (flat or noisy traces of the controls for spontaneous activity: **fig. S9**; **fig. S10C**, right: black-amber rotation stimulus). Accordingly, the responses of individual flies and the corresponding population means had comparable waveforms/dynamics (*cf*. UV-flies' responses to amber-motion in **fig. S10A** and **fig. S11A**); the population means of course contained less noise.

For each genotype, **table S2** further presents the optomotor performance of flies in terms of the repeatability of their behavior; quantified as the average maximum signal-to-noise ratio (SNR_{max}) of individual flies' torque responses. Here, *SNR* was calculated in the frequency domain using all recorded responses from 4,000 point long data chunks with 50% overlaps (with Blackman-Harris-term window) as explained in *Signaling performance estimates* section, above. Naturally, the behaviorally most relevant frequencies in the torque responses must be around 0.5 Hz, as each field rotation was relatively slow and lasted 2 seconds (see above); in concordance, when the flies responded with yaw-torque their SNR_{max} was at frequencies < 1 Hz. Note, however, that if $SNR_{max} < 1$, this does not mean that the flies would not see the stimulus; it only means that the stimulus evoked highly variable responses.

Estimating motion vision spectral range. **Figure 4**, (**C** left panel, **D** and **E**) shows optomotor responses to a broad-band motion (spectrally white: 380-900 nm) of flies, in which motion vision received inputs only from a single spectral class. Together, these optomotor responses summed up the WT-response (**Fig. 4G**). Therefore, we could predict the spectral range of visual motion by summing up the spectral sensitivity functions (nomograms) of the corresponding photoreceptor inputs, after weighting them by their apparent contribution to the WT optomotor response**.** As the first approximation, we used the mean torque response of each fly population (**figs. S11B-C**) as the weighting factors (%) for the corresponding photoreceptor inputs:

- Overall, R1-R6s contributed 57.5% and R7/R8s 42.5% to the wild-type response.
- Whilst, R7/R8 inputs had the following normalized weights:
    - R8y(Rh6) 46%
    - R7y(Rh4) 21%
    - R7p(Rh3) 18%
    - R8p(Rh5) 15%

The spectral range of motion vision, MV_{lambda} can thus be predicted conservatively:
MV_{lambda} = 0.575*R1-R6 + 0.425*(R7/R8) = 0.58*rh1 + 0.19*rh6 + 0.09*rh4 + 0.08*rh3 + 0.06*rh5.
MV_{lambda} is then normalized by its maximum (**Fig. 4I**; gray dotted line).

However, since the nomograms of Rh3-Rh6 pigments overlap only partially (**Fig. 4H**), this linear weighting underestimates R7/R8 inputs, providing the lower limit for their predicted contribution. Conversely, when Rh3-Rh6 weights are taken as the maxima of their respective optomotor responses (scaled to 74% of the normalized Rh1 input), the correspondence between the prediction and the measured spectral sensitivity of WT LMCs becomes even closer (**Fig. 4H**; thick gray line); particularly, at the long-wavelength range (540-580 nm).

We also note that the used broad-band motion stimulus had a slightly reduced UV-range. Therefore, the contribution of R7p-cells (rh3) is likely further underestimated. This is also suggested by WT LMC voltage responses, which showed higher sensitivity to 300 and 320 nm pulses (**Fig. 4I**).

Testing motion discrimination improvement by R8y input. In these experiments (**Fig. 4H)**, the panoramic stripe field was illuminated by a narrow band ultra-bright UV-LED (365 nm), which stimulate R1-R7 photoreceptors. Tethered flying UV-fly generated robust optomotor responses to alternating 2 second left and right field rotations; the motion stimulus parameters were the same as listed above. Illumination was then dimmed until the fly's optomotor responses almost ceased. After collecting torque responses (8-s long traces; n = 5-8) to this very dim UV-motion stimulus, the amber illumination (peak: 595 nm; full-width: 560-620 nm), which is only visible for R8y photoreceptors, was added on the ongoing very dim UV-illumination. Again, we collected 40-64 s of resulting torque responses. Examples of the mean responses with and without amber-motion in one experiment are shown in **Figure 4I**. In each experiment, to quantify the relative improvement in a fly's motion discrimination by amber input, both the mean torque responses with and without amber-motion were normalized by the maximum mean response to UV-motion alone (**Fig. 4J**). Amber illumination strengthened the optomotor responses by 36.4% ± 16.2% (mean ± SD; 8/11 flies; P = 0.00038; t-test for mean >1). Data from three flies were not used; although in the first test their responses increased to amber-motion (24%-47%), this effect petered out and became negative in the following tests (˜6%-˜18%).

In vivo two-photon imaging

We imaged changes in neural activity (changing calcium signals) in lobula plate tangential cells (LPTCs) to front-to-back and back-to-front visual motion using a two-photon laser scanning microscope with 1 NA 20XW objective. A mode-locked Ti:Sapphire Mai Tai SP Laser tuned to 920 nm was used as excitation source. Fluorescence was collected by photomultiplier tubes after bandpass filtering by 525/50 nm emission filter. Image (approximately 90 x 90 pixels) was acquired with ImSpectorPro (v.4.0.117) software at 9-13 Hz rate. The laser intensity was kept below

50 mW (measured at the back aperture) to avoid heat-induced artefacts (*77*). Two-photon imaging was performed from LPTCs in UV-flies (**fig. S12** and **fig. S13**) or in transgenic flies, which had WT photoreceptor pigments (**fig. S14**). GCaMP3 (*44*) was expressed selectively in LPTCs of UV-flies using the 3A-Gal4 (*45*). In addition to our own observations, other *Drosophila* laboratories have also confirmed us that 3A-Gal4 gives variable LPTC expression. Therefore, although the physiological characterization of many cells, owing to their preferred directional motion selectivity, strongly suggests that some of the cells were so-called vertical system tangential neurons, we did not attempt to further identify them in **figure S12** and **figure S13**, instead they are simply indexed from left to right: Cell1, Cell2…etc.

The images were exported to ImageJ, and the fluorescence intensity variations were quantified after background subtraction. Calcium variations were calculated by subtracting the basal fluorescence (F_0, calculated as the mean intensity before the visual stimulation) to the observed intensity (F) and dividing the result to F_0 (DF/F).

Fly preparation. The fly was prepared for imaging experiments as described in (*78*). The fly was waxed to a 0.001-inch-thick folded stainless steel shim holder, which allowed access to the back of the fly's head through a 0.8 mm opening. A small hole was made on the cuticle, left side of the head. Connective tissue was removed to obtain optical access to the left LPTCs. To maximize their response to the visual stimulation, the legs and wings were free to move (*14*).

Visual stimulation. The stimulation arena was made of a transparent semi-cylinder. The fly was placed in the centre of the stimulation arena spanning 73.6° in azimuth and 180° in elevation. Black stripes (wavelength = 15°), printed stripe-pattern on a silver paper (to minimize autofluorescence and maximize reflectance) was moved under the semi-cylinder by a custom-built linear stepping motor system at variable speeds (in these experiments typically 90°/s), resulting in 6 Hz temporal frequency. The arena was illuminated by UV LED (full-width 385 ± 30 nm; 390 mW) or by amber LED (full-width 590 ± 40 nm; 75 mW). The stimulation device was controlled by Biosyst (*12*, *37*) and synchronized with ImSpectorPro. A fly saw stimulation that consisted of 5 s stationary pattern segment, followed by a 15 s segment of front-to-back movement. Another 5 s stationary pattern segment, after which the pattern moved 15 s back-to-front, followed by the final 5 s stationary phase.

Besides verifying R8 input in the motion detection system (**fig S12**), these experiments enabled simultaneous spatiotemporal monitoring of how groups of neighboring LPTCs encode unidirectional motion with responses of opposing polarity (**fig. S12** and **fig. S13**). Such push-pull representation of motion information may be used to improve motion discrimination signals for flight control.

Questions and Answers:

Why cannot any residual Rh1-opsins in R1-R6 photoreceptors of UV-flies explain their optomotor responses to long-wavelength stimulation?

This is because:

(i) *In vitro* patch-clamp experiments showed no detectable response of R1-R6 photoreceptors from UV-flies to wavelengths beyond 560 nm (sensitivity at least 10^{8-9} times less than their UV-sensitivity; **Fig. 1C**). Furthermore, for amber stimuli, both UV-flies and *ninaE*^{8} mutants are at least 10^{6-7}-times less sensitive than wild-type R1-R6s (**Fig. 3G**). A million-fold loss of sensitivity beyond 500 nm means this is implausible.

(ii) In full agreement with the *in vitro* data, most of our *in vivo* recordings (~70%) from R1-R6 photoreceptor somata (in the retina of UV-flies) showed no detectable sensitivity to (>500 nm) stimulation - even when using maximally bright LED intensities (estimated to generate >10^{7} photons/s) (*e.g.* **fig S6A i** and **fig. S6**, **F** and **G**).

The amber motion stimuli, used in the flight simulator system (**figs. S9** to **S11**; **Fig. 4**) and during calcium imaging (**fig. S12** and **fig. S14**), were estimated to be 0.5-1.5 log-units dimmer than the amber LED stimuli used for the intracellular recordings. Thus, the amber motion detection ability of UV-flies or *ninaE*^{8} mutants necessitates contribution from R8 cells.

Why some R1-R6 photoreceptors of UV-flies respond to long-wavelengths with hyperpolarization or depolarization?

The depolarizations are likely caused by accessory excitatory inputs. Because they rise rapidly after the stimulus onset and their spectral responsiveness follows the spectral sensitivity of either R8y or R8p photoreceptors (as previously measured in other fly species (*71*)), this input should arrive to R1-R6 photoreceptors through functional contacts from R8 photoreceptors (**fig. S5A**). In dipteran flies, gap-junctions connect R6 to R8 photoreceptor axons at the distal face of the lamina (*28*, *29*) (**fig. S7**, **A** and **B**); these functional contacts are likely to channel R8-input into R6 cells (**Fig. 3J**). Furthermore, as all R1-R6 photoreceptor axons of are connected by gap-junctions (*29*, *36*) (**fig. S7D**), this input should spread to the other photoreceptors.

The hyperpolarizations are likely caused either by increased inhibitory or reduced excitatory inputs (**fig. S5A**). Because they are more delayed in respect to the given long-wavelength stimuli than the depolarizing responses of the same cells (to other wavelengths), their origin is most likely synaptic; presumably channeled from neighboring interneurons or glia (*30*, *79*). For example, the faster onset of the depolarizing responses in some LMCs suggests (Fig. 2C) that the hyperpolarizing input to R1-R6 cells could be driven by such depolarizations. Feedback synapses from interneurons and glia to R1-R6 are well-known in EM sections (*30*, *79*), many of which are likely to use excitatory transmitters (*80*, *81*). Physiological characterization of excitatory synaptic feedbacks from L2 monopolar cells to R1-R6 photoreceptors (*82*) suggests that these feedbacks are excitatory and tonically active. This connectivity means that when L2 cell hyperpolarizes, its tonic excitatory input to R1-R6s is reduced, causing R1-R6s to hyperpolarize.

Nonetheless, there could still be many other contributing connections due to the complex connectivity/interactions of many cell types in the retina and lamina (and medulla feedback).

Why only ~30% of R1-R6 photoreceptors of UV-flies exhibit R8-like sensitivity?

Because of coupling via gap junctions in the photoreceptors of lamina cartridge (*28*, *29*), one expects to find a spread of R8-like sensitivity to all photoreceptors with a magnitude that depends on the number of gap-junctions separating that cell from R6 (as suggested in **fig. S7**). However, only ~1/3 of our photoreceptor recordings showed responses to >500 nm. This discrepancy likely reflects chance differences in the recording stability and locations (somatic vs. axonal), because in UV-flies and *ninaE*^{8} mutants, the success of detecting accessory R8-like sensitivity in R1-R6 photoreceptors correlated positively with two factors:

(i) The quality of the microelectrode penetration.

The largest voltage responses to amber/green light were recorded in cells that showed low membrane potential (<-65 mV), high membrane impedance (>250 MΩ) and little instrumental noise; such as the recordings shown in **figure S6**. This suggests that signal leakage or noise in lower quality recordings make it harder to detect these gap-junctional inputs, back-propagating from the lamina.

(ii) The recording location, close to (or at) the lamina.

In the retina of *ninaE*^{8} mutants, we struggled to record light-induced responses from R1-R6 somata, although we observed low resting potentials, suggesting successful intracellular penetrations. With faulty Rh1-receptors making their phototransduction dormant, it was very difficult to locate the receptive fields of the cells, which now could only respond with residual R7/R8 signals, back-propagating from the gap-junctions in the lamina. Therefore, all presynaptic responses of *ninaE*^{8} mutants were likely recorded from the R1-R6 axons close to or within the lamina where these signals presumably originate (*28*, *29*) and thus should be larger. This recording location was identified by the distinctive alternation of depolarizing (R1-R6) and hyperpolarizing (LMC) responses as the electrode travelled through the tissue (*13*). Moreover, the responses of photoreceptors typically showed prominent initial transients to light onset (**fig. S5C**), characteristic of axonal penetrations (*83*).

These observations suggest that the largest responses (>30mV) to amber light (*e.g.* **Fig. 3**, **D** and **E**; **fig. S6F**) were likely recorded close to the lamina from R6 photoreceptors, which make direct gap-junctions to R8-cells (*28*). Overall, these large responses were rare (n = 5 R1-R6s). Even if one had 100% success rate of always recording from R1-R6 in the lamina, the probability to penetrate a R6 cell with an accessory R8y-sensitivity is ~0.12 (1/6 x 7/10). In real experiments, with the added difficulty of properly accessing the narrow lamina and penetrating small photoreceptor axons, the probability is less than that.

Why is it assumed that both R8 and R7 connect to R6?

This assumption is based on:

(i) the published gap-junction counts (**fig. S7C**) (*28*) and the ultrastructure of the distal face of the lamina where R7 and R8 axons make contacts only with R6 and R1 axons before entering the lamina (**fig. S7A**). ~75% of the R7 and R8 contacts, as counted from the electromicrographs, were with R6 photoreceptors; with R7s forming less gap-junctions than R8s (**fig. S7C**) (*28*).

(ii) *in vivo* recordings from R1-R6 and LMC in *ninaE*^{8} mutants, which accordingly showed broad but variable spectral sensitivity from UV to amber light (**Fig. 3**,

H and **I**; **fig S5**, **C** and **D**), although the R1-R6 phototransduction is effectively nonexistent (**Fig. 3G**).

(iii) briefer response waveforms of R1-R6 photoreceptors and LMCs to monochromatic UV-stimulation in UV-flies that either had light-insensitive R7/R8s (**Fig. 3A** and **fig. S5B**). However, it is uncertain to what extent R7 and/or R8 are responsible for the temporal increase in response as both R7/R8s were simultaneously deactivated.

However, these observations were not verified by dye-injections to directly determine, which R1-R6 photoreceptors received R7/R8 inputs. This is because:

(i) obtaining high-quality intracellular recordings with high-impedance sharp microelectrodes from very small *Drosophila* photoreceptors is by itself challenging. To detect the relatively weak R7/R8 inputs, the electrode needs to be inserted close to the gap junction. This preferably requires impaling the axon, which is very narrow (≤1 µm), and necessitates the impaling electrode tip to be very sharp (approx 50 nm).

(ii) filling photoreceptors electrophoretically with the same electrode is even harder; dyes increase the electrode impedance further, thereby increasing the recording noise, reducing the useful signal range, making compensation unreliable and blocking the electrode tip frequently. Larger electrode tips could be used for filling cells, but these are not likely to be able to impale the fine axons near the gap junctions and so it would not be possible to identify their relative spectral voltage changes.

Why only a small fraction of LMCs depolarize to R8 input?

As the recorded neurons were not labeled, we cannot provide a definite explanation for this surprising observation. However, we can offer two hypotheses for it:

(i) These responses may have been inadvertently recorded from LMC axons close to the medulla, reflecting gap-junctional inputs from R8y to one class of LMCs. These signals may be undetectable in typical lamina recordings, as the low input impedance synaptic zone in the lamina should shunt signal back-propagation from the medulla terminals (*84*). If so, we suggest that such excitatory contacts could enhance motion discrimination by differentiating the temporal profile of signals in the off-channel (L2) (*11*, *26*, *27*) from that of the on-channel (L1), which would lack this extra input.

(ii) It is also conceivable, but less likely (as by volume L1 and L2 are clearly the largest targets in the lamina (*79*)), that these recordings were from interneurons that receive excitatory synaptic inputs from both an LMC (thus the polarity of their output follows mostly that of LMCs) and R8y cell (which thus would oppose that of LMCs). With short-wavelengths, LMC input wins; with long-wavelengths, R8y input wins.

In addition to possibly refining motion detection, these neurons communicate color opponency by representing short- and long-wavelength information along a classic “push-pull” coding rule, functioning both in excitatory or inhibitory fashion (*cf*. **Fig. 2Bii** vs. **Fig. 2Cii**). We note that the recent reconstructions of the lamina ultrastructure have revealed even more sophisticated interconnectivity between photoreceptors, interneurons and glia (*79*) than what was known previously (*30*). Therefore, it is quite possible that local representations of environmental light changes are reshaped in an activity-dependent manner based on new information from other photoreceptors and information stored in the network (*13*, *58*). Thus, neural outputs of LMCs may

simultaneously subserve multiple functions, reflecting adaptive, suboptimal or context-dependent coding of visual events, rather than only serving motion detection (see the discussion in *58*).

Why optomotor responses of ninaE^{8} flies to amber-motion (Fig. 4B), which stimulates their R8y(Rh6) receptors only, are smaller than those of norpA Rh6 rescue flies to broadband-motion (Fig. 4D)?

In **Figure 4B** (*ninaE^{8}*), amber stimulus (560-620 nm) covers only a fraction (15-20%) of Rh6 spectral sensitivity range; the same input evokes relatively small LMC voltage responses (**Fig. 3I;** x-error bar). Conversely, in **Figure 4D** (*norpA* Rh6 rescue), the broadband stimulus (380-900 nm) covers Rh6 spectral range practically fully (100%; 99%-bounds: 340-660 nm). However, we further estimate that the intensity of the given amber-motion wavelengths (560-620 nm) was 2-3-times higher than the intensity of the same wavelengths (560-620 nm) in the broadband-motion. These differences between the amber- and broadband-motion stimuli probably go some way to explain the amplitude differences of the obtained optomotor responses.

Supplementary Tables and Figures

Table S1. Mutants used in the past for dissecting color and motion signals in *Drosophila*

Mutant/Transgenic	Description	Experimental Test
***sevenless* (*sev*^{1} *or* *sev*^{LY3})**	Degenerates photoreceptors R7.	Behavior, physiology. Homozygous animals sev^{4} lack UV phototaxis (*17*).
***ora transientless* (*ort*^{1})**	No receptors for histamine, the main neurotransmitter for R1-R8 photoreceptors, R1-R6 rhabdomeres slowly degenerate and are essentially absent after 14 days (*85*).	Impaired phototaxis (*17*).
***Rhodopsin1* (*ninaE*^{17})**	Degenerate photoreceptors R1-R6.	Retains about 12% of the normal course control and about 58% of the object fixation of normal flies when tested in fixed flying and freely walking assays (*86*).
***Hdc*^{JK910}**	*Histidine decarboxylase* null mutant.	Forms the correct number of synapses per presynaptic terminal independently of cartridge composition (*87*).
***norpA*^{36}**	phospholipase C null mutant (no receptor potential A); no phototransduction in all photoreceptors, rapid retinal degeneration, being more prominent in R1-R6.	Almost devoid of photoreceptor cells by day 10 (*88*). Forms the correct number of synapses per presynaptic terminal independently of cartridge composition (*87*).
***ora*^{JK84} = *ort*^{1}, *ninaE*^{1}**	Degenerates photoreceptors R1-R6 and disables the receptors for histamine, the main neurotransmitter for R1-R8 photoreceptors.	Impaired optomotor response and object fixation (*86*).
UAS-*shi*^{ts1} (*64*)	Potentially impairs synaptic vesicle recycling when over-expressed, altering vesicle release. Extremely deleterious for *Drosophila* photoreceptors (*46*).	Crossed to various Gal4 drivers for optomotor tests (*18*) and expressed in photoreceptors for color preference phototaxis assays (*9*).
Ort-Gal4	Targets neurons with histamine receptors using upstream sequence from the transcription start site of the ort gene (*90*).	Used in optomotor assays to determine contribution of L1 and L2 postsynaptic visual neurons (*18*).
GMR-Gal4	Expression of Scer\GAL4 is driven by five copies of the glass multimer reporter (GMR) in all cells posterior to morphogenetic furrow (*91*), including all eye photoreceptors. Some construct versions will cause a rough eye phenotype in the absence of a UAS driver when raised at 25 ^{o}C (*91*, *92*). Even constructs that appear wild-type could still rescue spitz mutants (*91*), indicating Gal4 over expression defects.	Probably the most widely used construct used for eye expression testing. Selected examples of GMR-Gal4 use include over expression of shibire in photoreceptors (*46*), over expression of tetanus toxin (*93*), labeling visual circuits (*94*), interrupting male aggression (*95*), understanding eye development (*96*). Studies using this driver are generally restricted to development, as its expression level from late-pupal to adult stages is low.
UAS-*ort*	Allows the expression of *ort* receptors in specific neurons using a Gal4 driver line in an otherwise mutant *ort* background (*90*).	Used in optomotor assays to determine contribution of L1 and L2 postsynaptic visual neurons (*18*).
***w*^{1118}**	White mutants do not produce screening pigments and therefore have white eyes. This common background, used to visualize mini-white P-element expression, often contains an Rh6 mutant with a 19-bp deletion that causes a stop codon to come in frame (*97*, *98*).	This white background is used in many different types of behavioral and imaging assays.

***rosy* (*ry*^{506})**	Has defective production of xanthine dehydrogenase resulting a deficiency of red pigment in the retina (*99*) and a shorter life span (*100*).	This mutation is often found on the same chromosome as *ninaE*^{17} and has been used in a range of behavioral and imaging assays.
***ebony* (*e*^{s} or *e*^{1})**	Has darker body pigmentation, altered circadian rhythm (*101*) and altered neurotransmission in visual system neurons (*102*, *103*).	The *ebony*^{sooty} mutation is often found on the same chromosome as *ninaE*^{17} and has been used in a range of behavioral and imaging assays.

Table S2. Optomotor performance metrics of different *Drosophila* genotypes used in this study for dissecting the reproducibility of their torque responses to black-white and black-amber field rotations (see **Fig. 4; figs S9-11**). Mean p-value for each genotype and treatment are given. Note, that if SNR_{max} < 1, this does not indicate that the flies would not see the stimulus; it only means that the stimulus evoked highly variable responses.

Genotype	**Stimulus: 380-900 nm**; 45 °/s, 14 ° black-white stripes, unit contrast		**Stimulus: 560-620 nm**; 45 °/s, 14 ° black-amber stripes, unit contrast	
	Testing whether a fly's responses were consistently > the chance level. Significant torque responses (10/10) in 10 trials ($p \leq 0.05$)	**Quantifying signal to background variation in the torque responses** SNR_{max} ≤ 1 Hz; mean ± SD (flies)	**Testing whether a fly's responses were consistently > the chance level.** Significant torque responses (10/10) in 10 trials ($p \leq 0.05$)	**Quantifying signal to background variation in the torque responses** SNR_{max} ≤ 1 Hz; mean ± SD (flies)
WT Canton-S	9/10 flies ($7*10^{-6} < p < 0.03$)	0.93 ± 0.44 ($n = 10$)	9/10 flies ($1*10^{-7} < p < 0.005$)	2.54 ± 1.95 ($n = 10$)
WT with inactive R7/R8 *norpA*^{36} R1-R6 *Rh1* rescue	8/10 flies ($1*10^{-6} < p < 0.04$)	1.26 ± 0.89 ($n = 10$)	-	-
WT with inactive R1-R6 *ninaE*^{8}	10/10 flies ($3*10^{-8} < p < 0.01$)	1.87 ± 1.32 ($n = 10$)	2/10 flies ($0.004 < p < 0.006$)	0.31 ± 0.17 ($n = 10$)
UV-fly *[Rh1 +3]; ninaE*^{8}	10/10 flies ($3*10^{-6} < p < 0.002$)	1.65 ± 0.66 ($n = 10$)	2/10 flies ($0.009 < p < 0.01$)	0.24 ± 0.13 ($n = 10$)
UV-fly with Ca^{2+}-sensors in LPTNs *[DB331]; [CAM2]; [Rh1+3]; ninaE*^{8}	12/12 flies ($1*10^{-16} < p < 0.03$)	4.58 ± 5.49 ($n = 12$)	4/11 flies ($5*10^{-4} < p < 0.05$)	0.30 ± 0.13 ($n = 10$)
UV-fly with Ca^{2+}-sensors in LPTNs *[DB331]; [GCaMP3]; [Rh1+3]; ninaE*^{8}	5/5 flies ($1*10^{-6} < p < 0.01$)	1.72 ± 0.68 ($n = 5$)	-	-
UV-fly with inactive R7/R8 *norpA*^{36} R1-R6 *Rh3* rescue	4/6 flies ($8*10^{-3} < p < 0.04$)	0.77 ± 0.25 ($n = 6$)	0/6 flies only spontaneous activity	0.26 ± 0.07 ($n = 6$)
Only R7p active *norpA*^{36} R7p *Rh3* rescue	1/10 flies ($p < 0.05$)	0.30 ± 0.19 ($n = 10$)	-	-
Only R7y active *norpA*^{36} R7y *Rh4* rescue	1/10 flies ($p < 0.01$)	0.33 ± 0.31 ($n = 10$)	-	-
Only R8p active *norpA*^{36} R8p *Rh5* rescue	2/10 flies ($0.02 < p < 0.05$)	0.20 ± 0.14 ($n = 10$)	-	-
Only R8y active *norpA*^{36} R8y *Rh6* rescue	9/10 flies ($2*10^{-4} < p < 0.04$)	0.84 ± 0.61 ($n = 10$)	-	-

Fig. S1. Photoreceptor rhabdomere structure in mutant and UV rescue *Drosophila*. (**A**-**H**). Tangential sections through genotypes 5 days post-eclosion, taken immediately below the rhabdomere cap. R3 photoreceptors are indicated with an asterisk. (**A**) Wild type Canton-S (**B**) Rescue of *ninaE*^{8} using [Rh1+3] from Charles Zuker. Note that *ninaE*^{8} have intact but reduced R1-R6 rhabdomeres (*33*). (**C**) *ry*^{506}, *ninaE*^{17}, *e*^{s} are the most commonly used mutant strain for dissection of visual circuits (**D**) [Rh1+3] rescue of *ry*^{506}, *ninaE*^{17}, *e*^{s}. Rhabdomeres are obviously elongated, twisted in orientation and misplaced directly below the lens above when compared with wild-type. (**E**) This *ninaE*^{17} mutant was recently made by removing the rosy and ebony markers by recombination in Japan (*54*). (**F**) [Rh1+3] rescue of *ninaE*^{17} from Japan. (**G**) This [Rh1+3] rescue of *ninaE*^{8} also had expressed DB331-Gal4 that targets the lobular plate and UAS-TNXXL a troponinC FRET based genetically encoded calcium indicator. (**H**) These totally UV sensitive flies have *ninaE*^{8} rescued with [Rh1+3], along with *norpA*^{36} rescued with [Rh1+*norpA*], in addition to also having DB331-Gal4 and UAS-TNXXL. Note the R7 is fully intact despite having no color response.

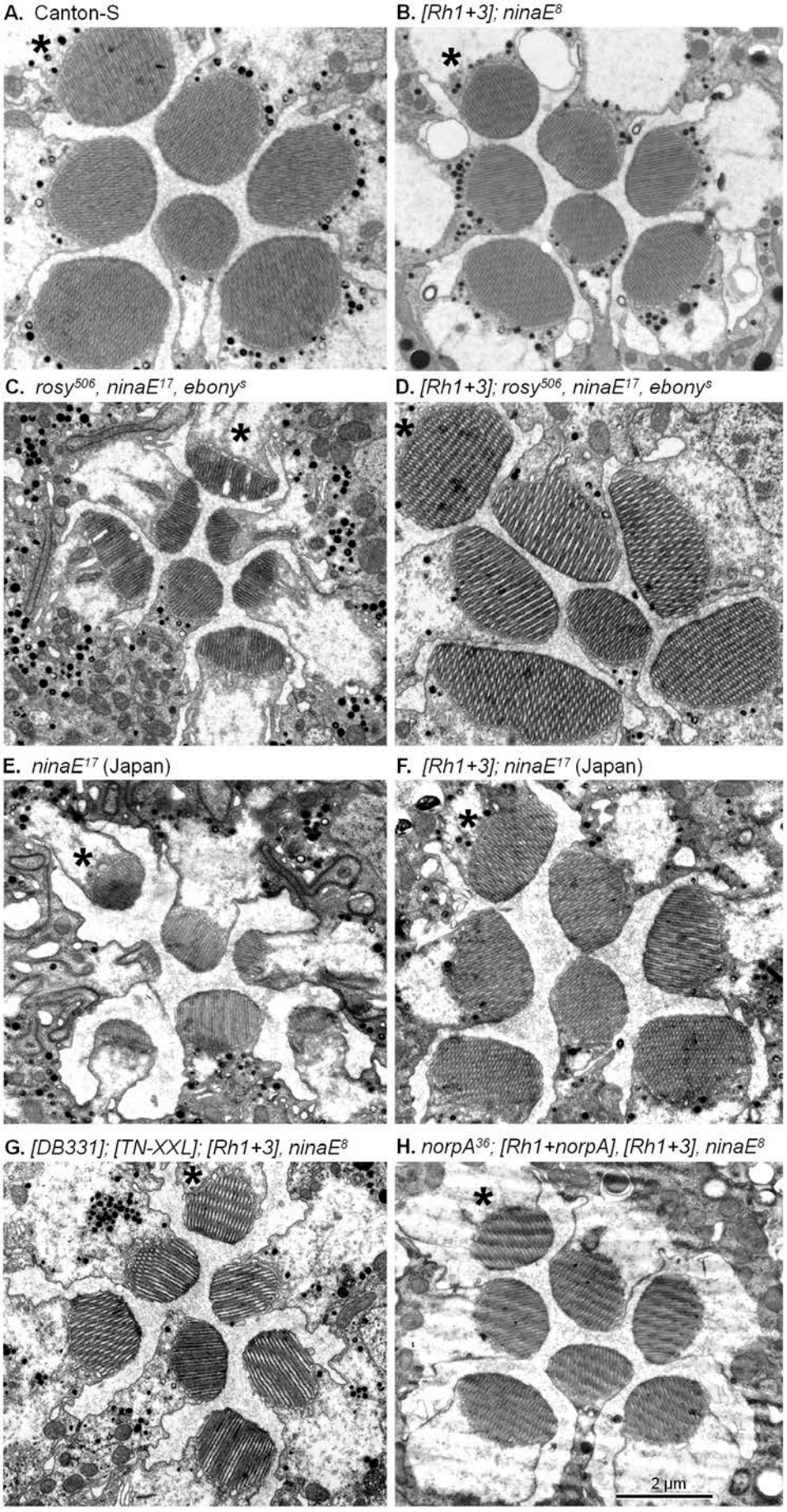
A. Canton-S
B. [Rh1+3]; ninaE8
C. rosy506, ninaE17, ebonys
D. [Rh1+3]; rosy506, ninaE17, ebonys
E. ninaE17 (Japan)
F. [Rh1+3]; ninaE17 (Japan)
G. [DB331]; [TN-XXL]; [Rh1+3], ninaE8
H. norpA36; [Rh1+norpA], [Rh1+3], ninaE8
2 µm

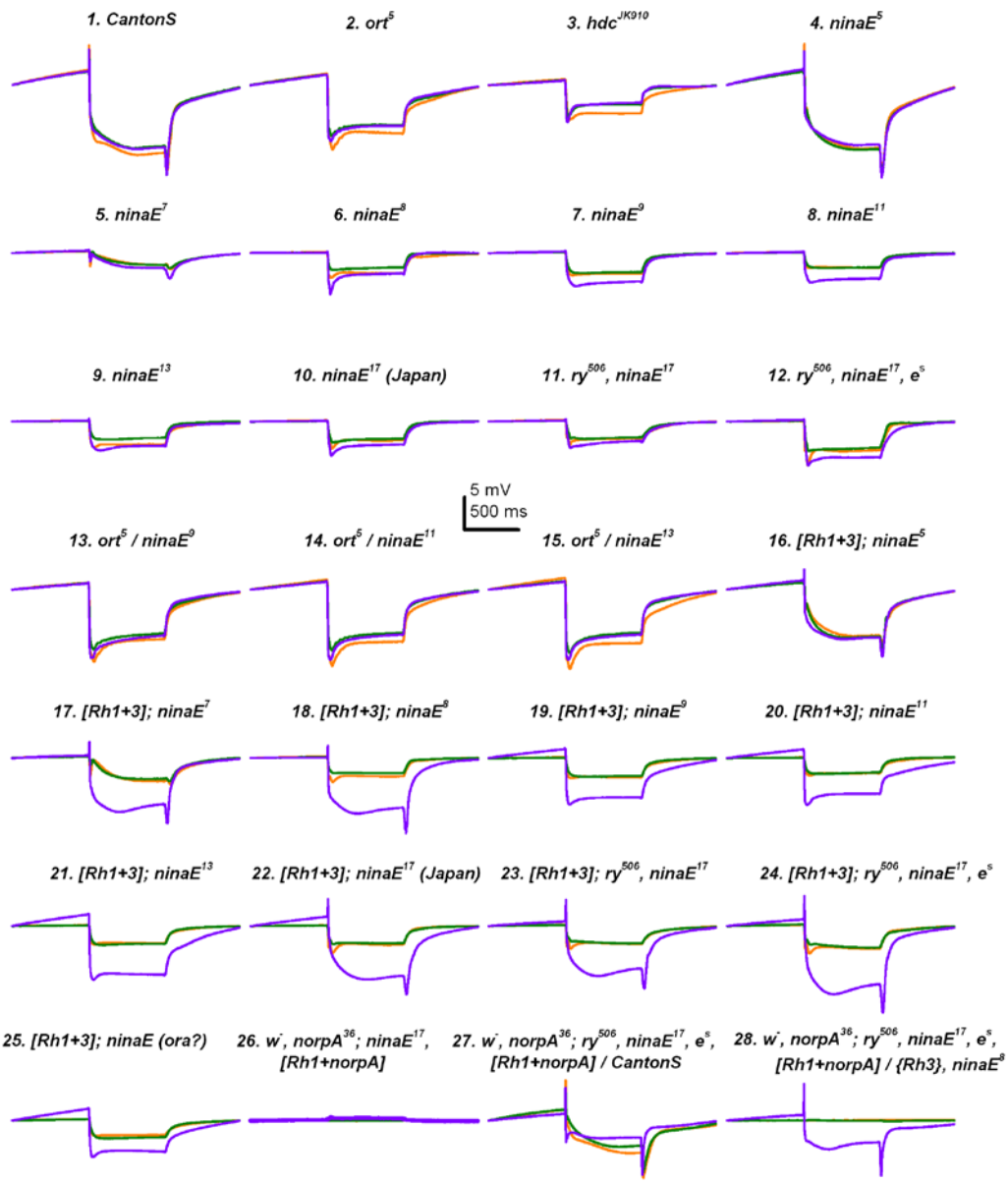

Fig. S2. Electroretinogram (ERG) waveforms from numerous mutant and rescue *Drosophila* that were previously dark adapted for 3 minutes. Illumination: 700 ms pulses from high power LEDs (purple: 385 ± 30 nm, green: 505 ± 35 nm, amber: 595 ± 40 nm). Each trace represents the mean response from five flies (5 days post-eclosion), from the mean of responses 5-10 delivered to each fly. (1) Wild type ERG response. (2) ort^{5} lacks the histamine receptor, therefore is missing the typical on- and off-transients. (3) Hdc^{JK910} is unable to produce histamine, cannot adapt to light and has lower photoreceptor responses, but can easily be fully rescued when fed histamine. (4-12) ERG responses from *ninaE* mutants; $ninaE^{8}$ appears most similar in size and speed to Hdc^{JK910} indicating proper photoreceptor function (13-15) Heterozygote ort^{5} and *ninaE* flies, revealed three *ninaE* mutants also contained *ort*. (16-24). Rescuing *ninaE* mutants (4-12) with Rh3 revealed that $ninaE^{8}$ also had normal neurotransmission. (25) Two *ninaE* stocks, obtained from vision research labs and used for publication, were also found to contain *ort*. (26) Rescue of *norpA* in a *ninaE* background reveals absent ERG waveform (27) Genetic control showing WT R1-R6 ERG responses with R7-R8 being light-insensitive. (28) UV-Fly with light insensitive R7/R8 receptors. Genotypes 26-28 were homozygous for the $white^{1118}$ mutation. Flies homozygous for

rosy^{506} or *ebony*^{sooty} had abnormal ERG responses, which were typically slower and poor in photoreceptor adaptation.

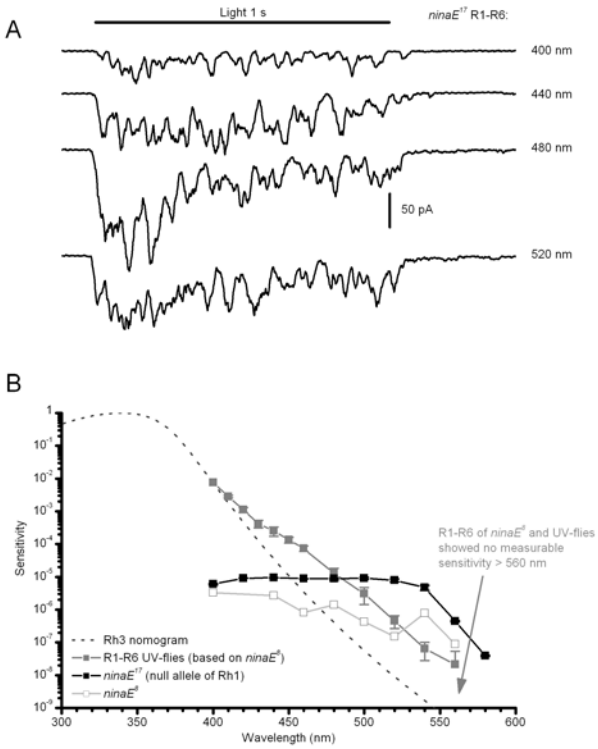

Fig. S3. Comparing spectral sensitivities of R1-R6 photoreceptors in *ninaE* mutants and UV-flies. (**A**) In whole-cell patch-clamp, dissociated R1-R6 photoreceptors of *ninaE*^{17} mutants, having a null-allele of blue-green Rh1 opsin (*ninaE*), generated noisy light-induced current backgrounds to a range of wavelengths. (**B**) The spectral sensitivity of *ninaE*^{17} is ~10-times higher than that of *ninaE*^{8} photoreceptors, which generated maximally 1-2 bumps/s to the same stimuli. The responsiveness of *ninaE*^{8} photoreceptors was too low for measuring reliably their spectral sensitivity over the range of wavelengths; they had larger bumps than *ninaE*^{17}, and consequently their sensitivity is overestimated here. The light gray line gives an approximation of their sensitivity, integrated in the same way as that of *ninaE*^{17}. Our UV-flies were based on *ninaE*^{8} mutant by expressing an ultra-violet opsin (Rh3) (*32*) in R1-R6 photoreceptors. The spectral sensitivity of these photoreceptors were up to 50-fold less sensitive than *ninaE*^{17} photoreceptors at the long-wavelength range (480-600 nm) but also less sensitive than *ninaE*^{8} R1-R6s at wavelengths >520 nm. This suggests that over-expression of Rh3 in these cells may suppress any residual opsin expression. At wavelengths >560 nm R1-R6 photoreceptors of UV-flies and *ninaE* mutants did not respond to the given bright stimuli of our monochromator system. Mean ± SD shown. *ninaE*^{17}, n = 2 cells; *ninaE*^{8}, n = 2 cell; UV-flies, n = 3 cells.

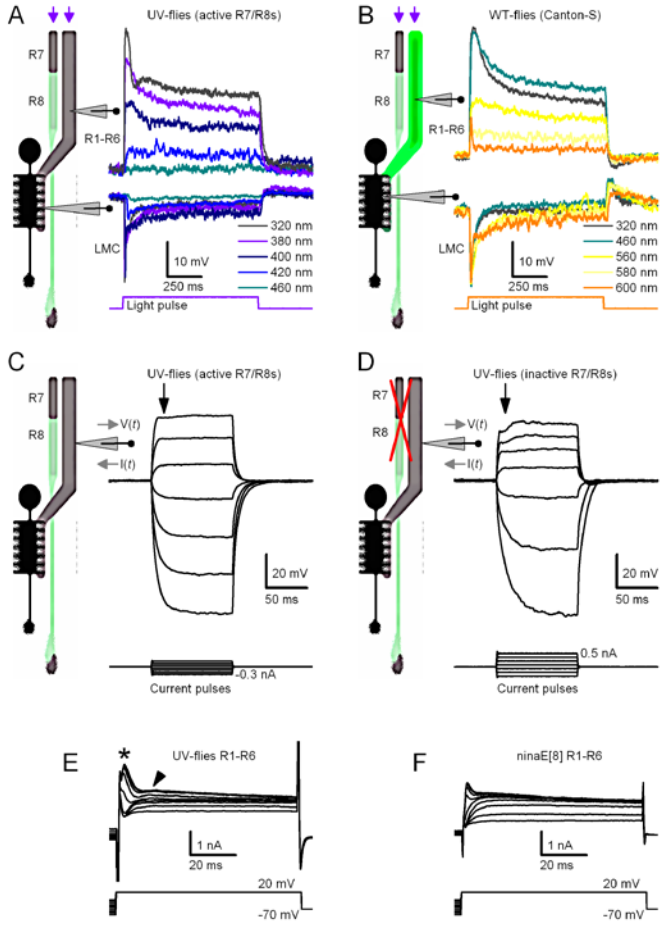

Fig. S4. Pre- and postsynaptic response dynamics in UV-fly retina/lamina *in vivo* are WT-like. (**A**) Intracellular voltage responses of a R1-R6 photoreceptor and a LMC to 700-ms color pulses, recorded from two UV-flies, respectively. This particular UV-fly also expressed calcium-reporter GCaMP3.0 in the lobula plate tangential vs-cells, indicating that this genetic manipulation had little influence on synaptic photoreceptor output at the level of lamina. Typically post-synaptic recordings show variable degrees of off-response, possibly attributable to different LMCs: L1 (on-channel) or L2 (off-channels) (*11*). Responses illustrate how sensitivity and speed of adaptation diminish with increasing stimulus wavelength. Dynamics match those in WT phototransduction (*12*) and synaptic transmission *in vivo* when photoreceptors' photon capture reduces (*13, 58*, *62*). Notice how summation of larger and fewer elementary responses (bumps) make R1-R6 output noisy during longer wavelength inputs, implying normal bump adaptation (*12*). (**B**) Similar recordings as in (A), but to different colors from two WT-flies. Comparable response dynamics in UV- and WT-flies indicate preserved circuit computations in the lamina. (**C**) Representative voltage responses of a R1-R6 to current pulses in a dark-adapted UV-fly. (**D**) Similar responses in an UV-fly, whose R7/R8s were light-insensitive (using a *norpA*^{36} mutant and a *norpA* rescue in R1-R6). In both cases (C and D), depolarizing current pulses caused outward rectification (black arrows) of the membrane; owing to activation of shaker and delayed rectifier K^+-channels, analogous to WT R1-R6s (*12, 66, 104*). Their characteristic dynamics and impedances (254 and 133 MΩ, respectively) are within the normal variation of WT recordings (*12, 66, 104*), indicating normal R1-R6 plasma-membranes.(**E**) In whole-cell patch-clamp, dissociated R1-R6 photoreceptors of UV-flies showed normal-like K^+-currents with characteristic shaker and shab components (*105*). (**F**) Similarly, R1-R6 photoreceptors of *ninaE*^{8} mutants, showed large K^+-currents, having both Shaker (asterisk) and Shab (arrow note arrow here also shows putative ShaI current) components; the UV-flies were derived from this stock.

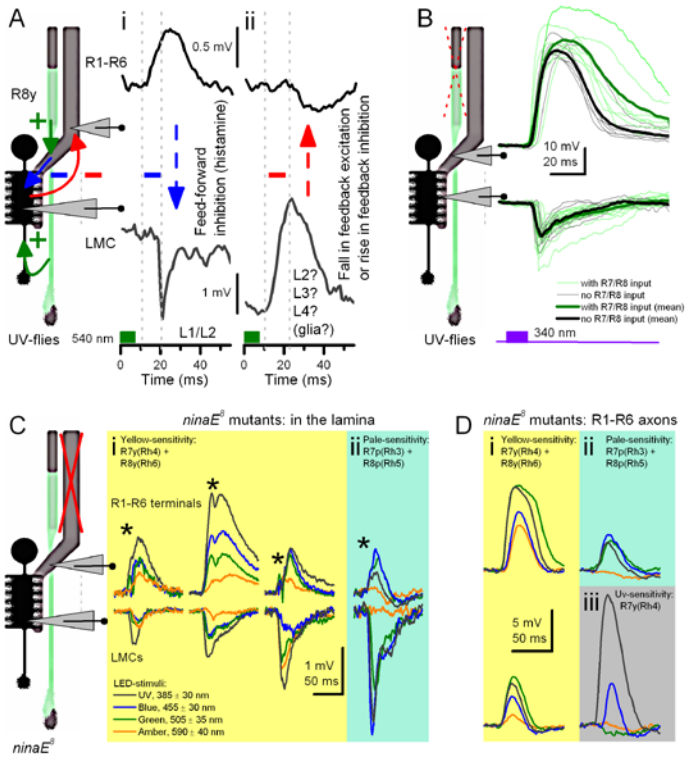

Fig. S5. Within the first optic neuropile (lamina), information from R7/R8 cells is spread to R1-R6 photoreceptors and LMCs in a push-puller manner, shaping their voltage responses. (**A**) *in vivo* intracellular voltage responses of R1-R6 photoreceptors and LMCs to a sub-saturating 10-ms-long monochromatic pulse (540 nm), each recorded from different UV-flies. Green-yellow stimulation can evoke depolarizing or hyperpolarizing responses in some R1-R6 photoreceptors (~30%) of UV-flies, and hyperpolarizing or depolarizing responses in all LMCs (100%). Correlating the time courses of the pre- and postsynaptic responses suggest that: (**i**) Fast rising depolarizing photoreceptor output (from R8 cells via gap-junctions) is sufficient to drive feed-forward histaminergic transmission to LMCs, hyperpolarizing them. (**ii**) Depolarizing LMC output proceeds hyperpolarizing R1-R6 output, indicative of synaptic feedback transmission. Either fall in feedback excitation or rise in feedback inhibition, as mediated by network connections, could selectively hyperpolarize some R1-R6s. (**B**) Intracellular voltage responses from R1-R6 photoreceptors and LMCs in UV-flies with normal light-sensitive R7/R8 photoreceptors (green lines) or with light-insensitive R7/R8s (black and gray lines). The stimulus is a very bright 340 nm monochromatic pulse, which apart from evoking normal saturating responses in the UV-sensitive R1-R6 cells should also stimulate R7 cells much more than R8 cells. Wider responses of R1-R6 photoreceptors and LMCs in UV-flies with light-sensitive R7/R8 cells suggest that R7 inputs would also shape R1-R6 outputs. This raw data was shown normalized in Figure 3A. Thick lines are the means, thin are responses of individual cells. (**C**) In *ninaE*^{8} lamina, depolarizing voltage responses of R1-R6 terminals to very bright (saturating) pulses (from LEDs) show broad spectral sensitivity from UV to amber light, combining the inputs of the specific R7/R8 pair, which shares their neural superposition. Similar spectral sensitivity is also obvious in the hyperpolarizing responses of LMCs. Notice how saturating light stimuli (of comparable intensity) generates 10-times smaller responses in *ninaE*^{8} R1-R6 axons than in R1-R6 somata of UV-flies (B). (**i**) Examples of similar recordings as in (A), from *ninaE*^{8} where most cells had R7y(Rh4) + R8y(Rh6) sensitivity and (**ii**) only one photoreceptor and LMC showed likely R7p(Rh3) + R8p(Rh5) sensitivity. Asterisks highlight the fast depolarizing transients that characterize recordings from photoreceptor axon terminals (*83*). (**D**) R1-R6 recordings close to (or at) the lamina (**i** and **ii**) show combined R7+R8 sensitivity, apart from two recordings, which had Rh4-sensitivity; one shown in (**iii**). Note that these responses to saturating pulses are 3-10-times smaller than those recorded in R1-R6 somata of UV-flies.

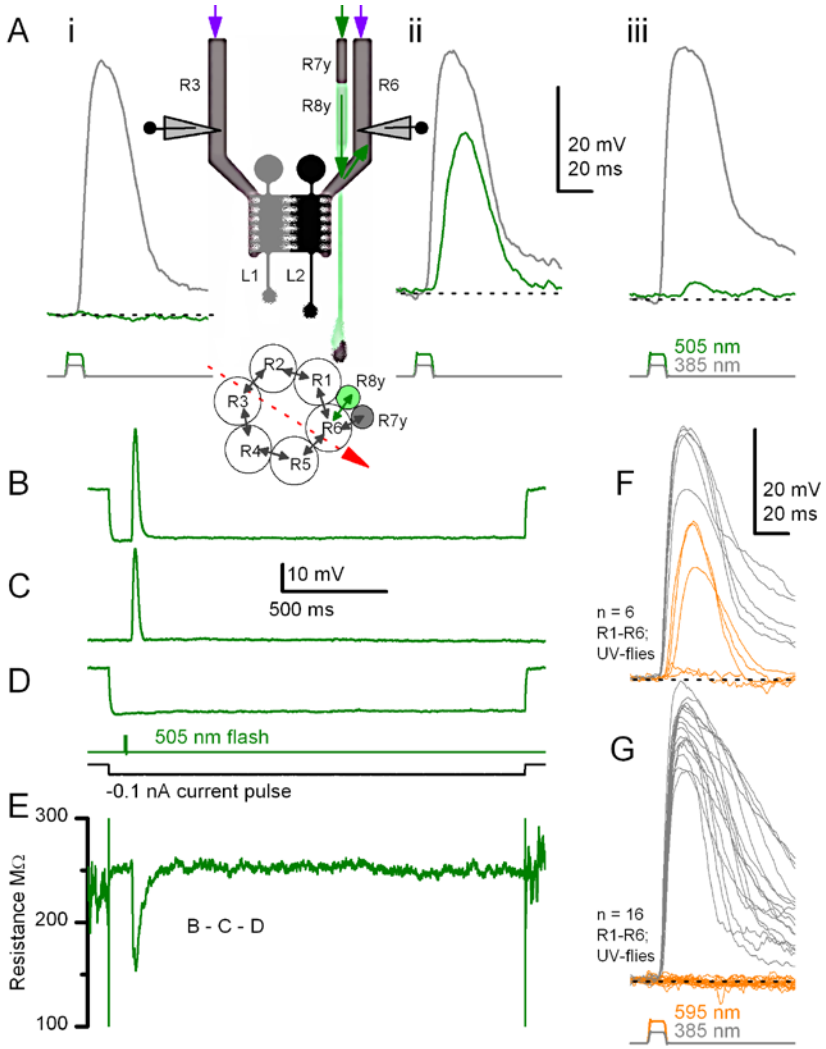

Fig. S6. Variable sensitivity and resistance changes in R1-R6 photoreceptors of UV-flies confirm that their responses to long wavelength saturating stimuli are neither recording artefacts nor field potentials. (**A**) Intracellular responses of different photoreceptors in the same fly to maximally bright UV and green-yellow flashes. (**i**) First cell responded to UV but not to green. (**ii**) Next cell (likely R6 in the same or neighboring neuro-ommatidium) responded to both UV and green. This cell cannot be R7y/p, which are less green-sensitive, or R8y/p, which are less UV-sensitive. Inset highlights a hypothetical recording path, somewhere close to the retina/lamina border (red arrow), and gap-junctions (black arrows) between photoreceptors (*28, 36*) (**iii**) Fifth cell responded to UV and weakly to green-yellow. Third and forth cells responded as cell (**i**) (**B**) Response to 10 ms green-yellow flash (as above) combined with current pulse (black), which hyperpolarized membrane potential to linear current-voltage range (*66*), in cell (**ii**). (**C**) Response to green-yellow flash without current pulse. (**D**) Response to current pulse without flash. (**E**) Responses of (C) and (D) subtracted from the response of (B). The resistance follows from voltage and current, its value when the photoreceptor is not illuminated. Drop in resistance, caused by conductance increase to yellow-green flash that UV(Rh3)-sensitive R1-R6s cannot see (**Fig. 1C**), implies gap-junctional inputs from the R8y-photoreceptor, viewing the same point in space (schematic in A). (A): single responses; (B-E): mean of ten responses. Shaw's map of electrically interacting responses in *Lucilia* neuro-ommatidia (**fig. S7)** (*29*) predicts diminishing R1-R6s' green-yellow sensitivity away from R8, consistent with our observations. Illumination from high power LEDs (gray: 385 ± 30 nm, green: 505 ± 35 nm). (**F**) Intracellular responses of six R1-R6 photoreceptors to maximally bright UV and amber (595 nm ± 40 nm) flashes. Each of the cells responded to amber (either by 1-2 mV transient blips or by large depolarizations). (**G**) Intracellular responses of

sixteen R1-R6 photoreceptors to the same stimulus as in (F). None of the cells responded to amber. Data in (**F** and **G**) are from the same 5 UV-flies.

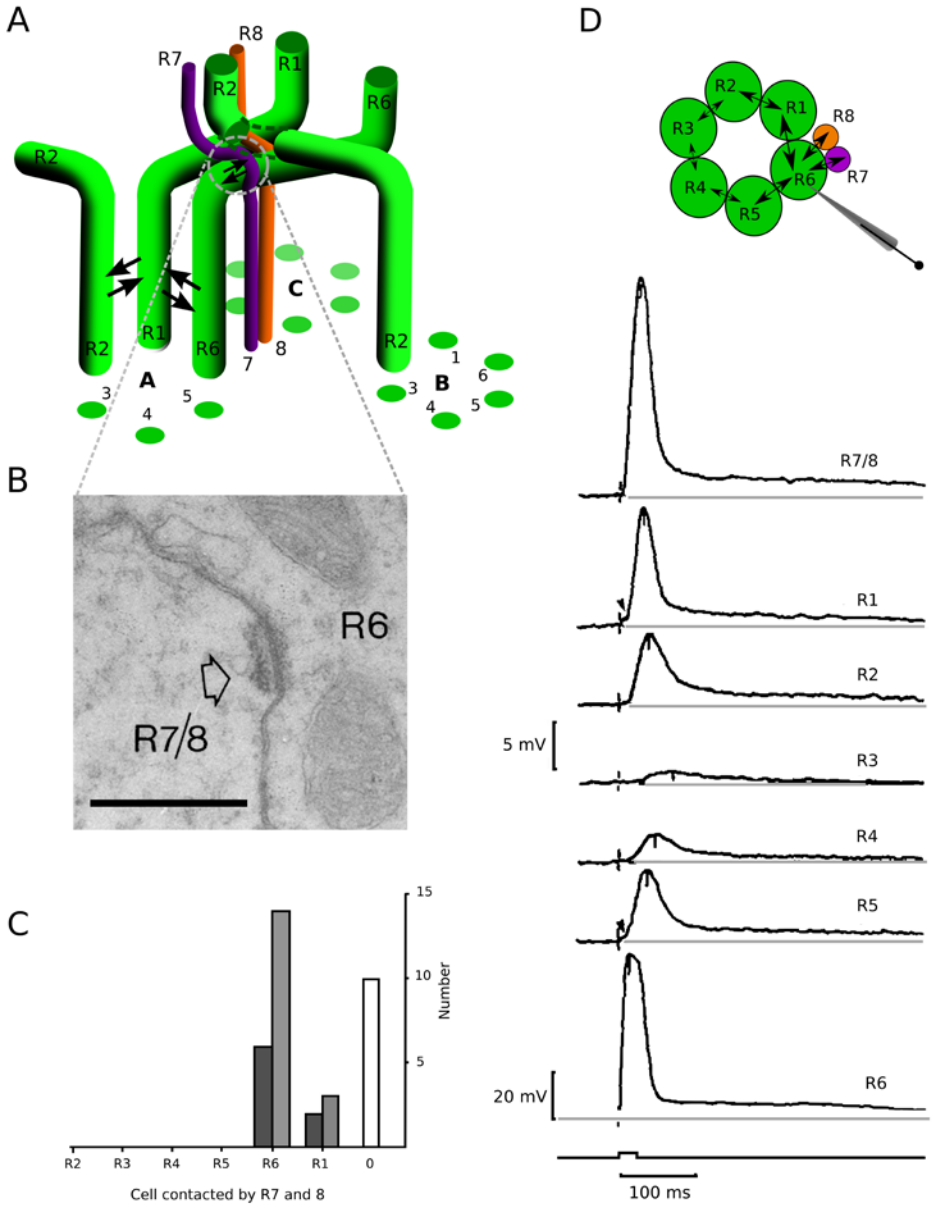

Fig. S7. Summary of results by Shaw, Fröhlich and Meinertzhagen, indicating functional contacts between R6 and R7/R8 photoreceptors in lateral eye region of *Lucilia*. (**A**) Diagram showing how receptor axons arrive at the distal face of the lamina. [A, B, C: R1-R6 terminals in three cartridges]. Arrows indicate local coupling between neighbours. R7 and R8 axons travel as a pair on either side of the R2, originating in their own ommatidium, and then part, leaving R6 axon between them. This pattern is repeated in all axon bundles entering the lamina in each half of the eye. (**B**) A putative gap junction showing obvious but asymmetrically distributed densities, more prominent in R7/8 (arrow) than in R6. x36,500, scalebar: 0.5 µm. (**C**) Frequency count for photoreceptor terminals of R1-R6 contacting R7 and R8 axon pairs. Counts have been scored from a photomontage in which the identities of R7 (dark gray) and R8 (light gray) have been inferred from their relative positions only. Blank bar (0) indicates cartridges in which neither profile happened to be found in contact with a R1-R6 terminal. (**D**) Tracing of signal averaged responses from the soma of a photoreceptor R6, identified from the position of its own facet in the map of electrically interacting responses plotted around it, using a roving fibre optic probe. The responses are attenuated versions of those of the corresponding terminals around R6 in its cartridges, mapped in (inset above). Responses R1-R5 illustrate the progressive reduction in the size of the response and the lengthening of time-to-peak, going away from R6 in both directions around the ring of terminals. The coupled responses

all show a miniature depolarizing afterpotential. Terminals nearest the recorded cell exhibit a 'notch' early on their rising phases (arrowheads). The largest coupled response in this map came from the R7/R8 input to this cartridge. Figures and legends adapted from Shaw (*29*) and Shaw, Fröhlich and Meinertzhagen (*28*) with permission.

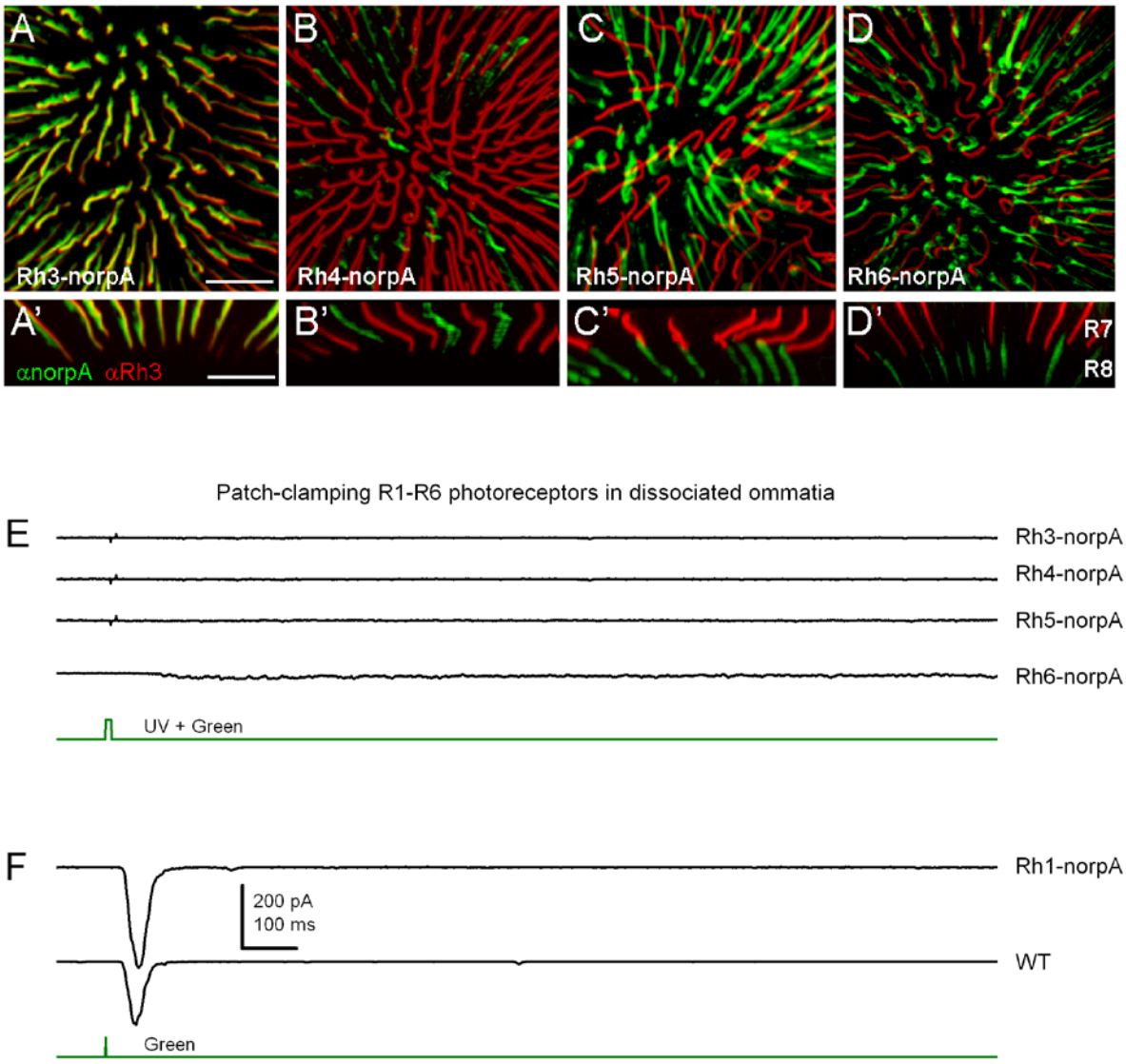

Fig. S8. *norpA* expression patterns in the retinas of rescued *norpA* flies and examples of whole-cell patch-clamp recordings from dissociated R1-R6 photoreceptors in these flies. (**A-D'**) Anti-*norpA* (green) staining of retinas. Specific opsin promoters were used to rescue norpA expression in different R7 and R8 subtypes in *norpA* mutant flies: (**A**) Rh3-*norpA* (for R7p); (**B**) Rh4-*norpA* (for R7y); (**C**) Rh5-norpA (for R8p); (**D**) Rh6-*norpA* (for R8y). (**A'-D'**) Horizontal views of (**A-D**). R7p photoreceptors labeled by anti-Rh3 antibody (red) were used as reference. Scale bar: 30 μm (**A, A'** for **A-D'**). In B and B', the y/p ratio is lower than in the other figures due to weaker anti-*norpA* labelling in a small region of the retina that was imaged. (**E**) Rh3-*norpA*, Rh4-*norpA*, Rh5-*norpA* and Rh6-*norpA* photoreceptors lack light-current responses to very bright pulses; light stimuli were several hundred-fold brighter than those is in F (below), including ultra-bright UV led as well as green LED for Rh3 and Rh4. These results clarify that R1-R6 Rh1-Rh4-*norpA* are virtually blind and that R7 or R8 photoreceptors do not make any functional contacts to them at the level of retina. Thus, the corresponding gap-junctions and synapses are located in the lamina, as shown in **Figure 2.** (**F**) Rh1-*norpA* and WT R1-R6 photoreceptors generate normal light-current responses to dim green flashes (ca. 100 effective photons). Representative of 3 cells for each genotype.

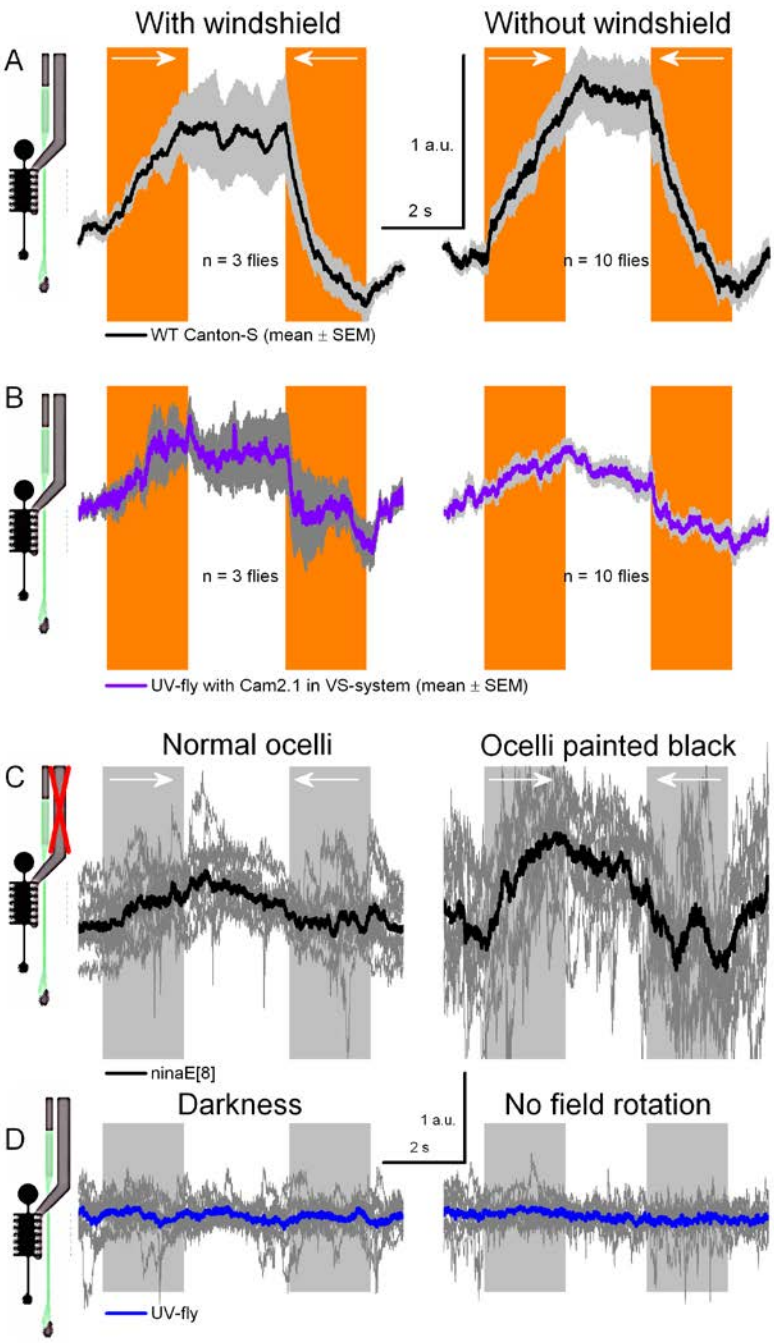

Fig. S9. Control measurements of optomotor behavior in the flight simulator system. (**A**) Optomotor responses of tethered flying wild-type *Drosophila* to black-amber stripe-field rotations (indicated by amber bars with the arrows pointing the directions of rotations) are similar with and without a windshield. (**B**) Optomotor responses of UV-flies to the same stimulus are similar with and without a windshield. Thick lines represent each mean, grey shading the SEM. (**C**) Covering occelli with black paint did not abolish optomotor behavior of *ninaE*^{8} mutants (having light-insensitive R1-R6 photoreceptors), verifying that R7 and R8 photoreceptors were sufficient to provide inputs for its motion detection system. (**D**) Optomotor behavior of WT-flies to rotation stimuli in darkness and with immobile visual field (black-white stripes). Thin lines represent individual responses and thick lines represent each mean. Notice the large degree of spontaneous activity, including fast saccades, with (C) and without (D) optomotor stimulus in each trial.

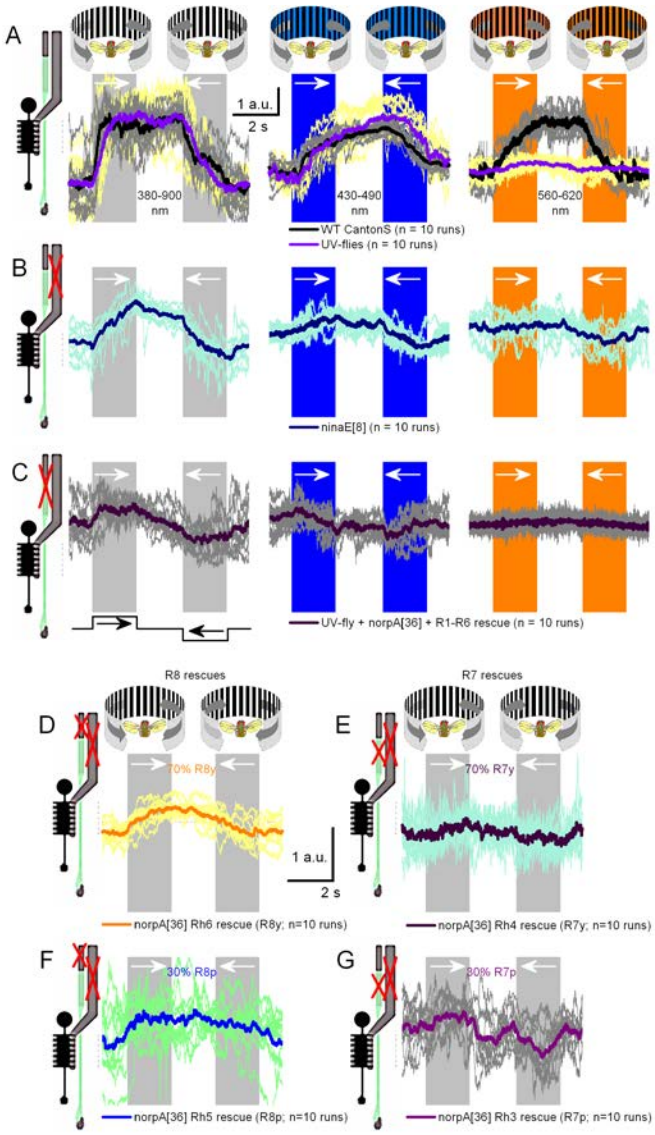

Fig. S10. Optomotor behavior of individual tethered flying *Drosophila* to 10 successive field rotations to left and right of the given color (black-white, black-blue or black-amber). (**A**) Both UV-flies (R1-R6s expressing Rh3-opsin) and wild-type react to broad spectral range of motions with systematic but variable torque responses. (**B**) Mutant *ninaE*^{8}-flies, having light-insensitive R1-R6 photoreceptors (*cf*. **Fig. 3G**; motion pathway) but normal R7/R8 photoreceptors, react to an equally broad spectral range of motions as in A. (**C**) *norpA*^{36}-flies, having R1-R6 photoreceptors rescued with Rh3 opsins, react to black-white and black-blue motions but not to black-amber motion. (**D** and **F**) Rescuing light-sensitivity only in R8y or R8p photoreceptors, respectively, enable visual motion perception. (**E** and **G**) Rescuing light-sensitivity only in R7y or R7p photoreceptors enable weak/noisy motion perception; see also **figs. S11B-C**.Thin lines represent individual responses and thick lines represent each mean.

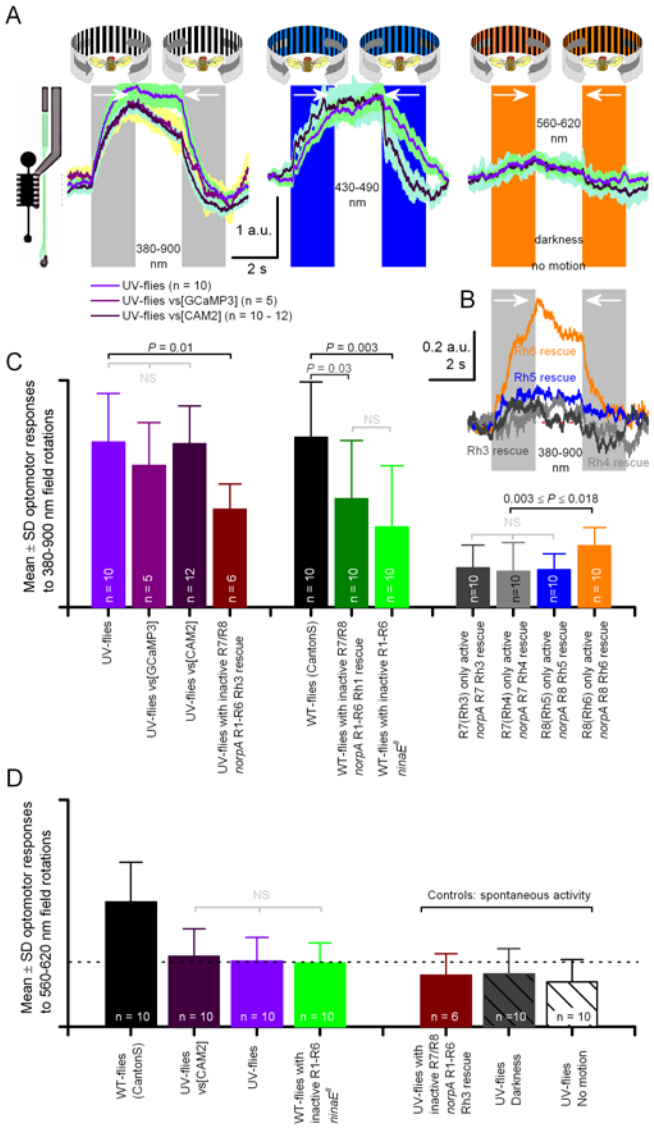

Fig. S11. Statistics for optomotor responses of different flies used in this study. (**A**) Comparison of the yaw-torque responses of UV-flies and UV-flies that express calcium reporters (either GCaMP3 or Camelion 2.1 = CAM2) in the lobula plate tangential vs-cells to right and left field rotations of different spectral content. The mean responses of these fly strains are similar, having characteristic dynamics for the three tested field rotations of different spectral ranges. (**B**) Mean torque responses of *norpA*^{36} flies with rescued light-sensitivity in R8y, R8p, R7y or R7p photoreceptors (n = 10) to spectrally broad motion stimuli. Each rescue enables visual motion perception. (**C**) Mean yaw-torque responses (the full range) of different flies used in this study to spectrally broad left and right field rotations. (**D**) Mean optomotor responses (the full range) of WT- and different UV-flies and *ninaE*^{8} mutants to amber left and right field rotations. Controls for spontaneous optomotor behavior: NorpA with Rh3-rescue in R1-R6 (normal amber motion stimuli); UV-flies in darkness (field rotation stimuli); UV-flies surrounded with the normal black-white field (no rotation). The hypothesis that the mean full range of optomotor responses in one genotype (*n* = 6-12 flies) is larger than that in the other genotype is tested; significance given by two-tail t-test.

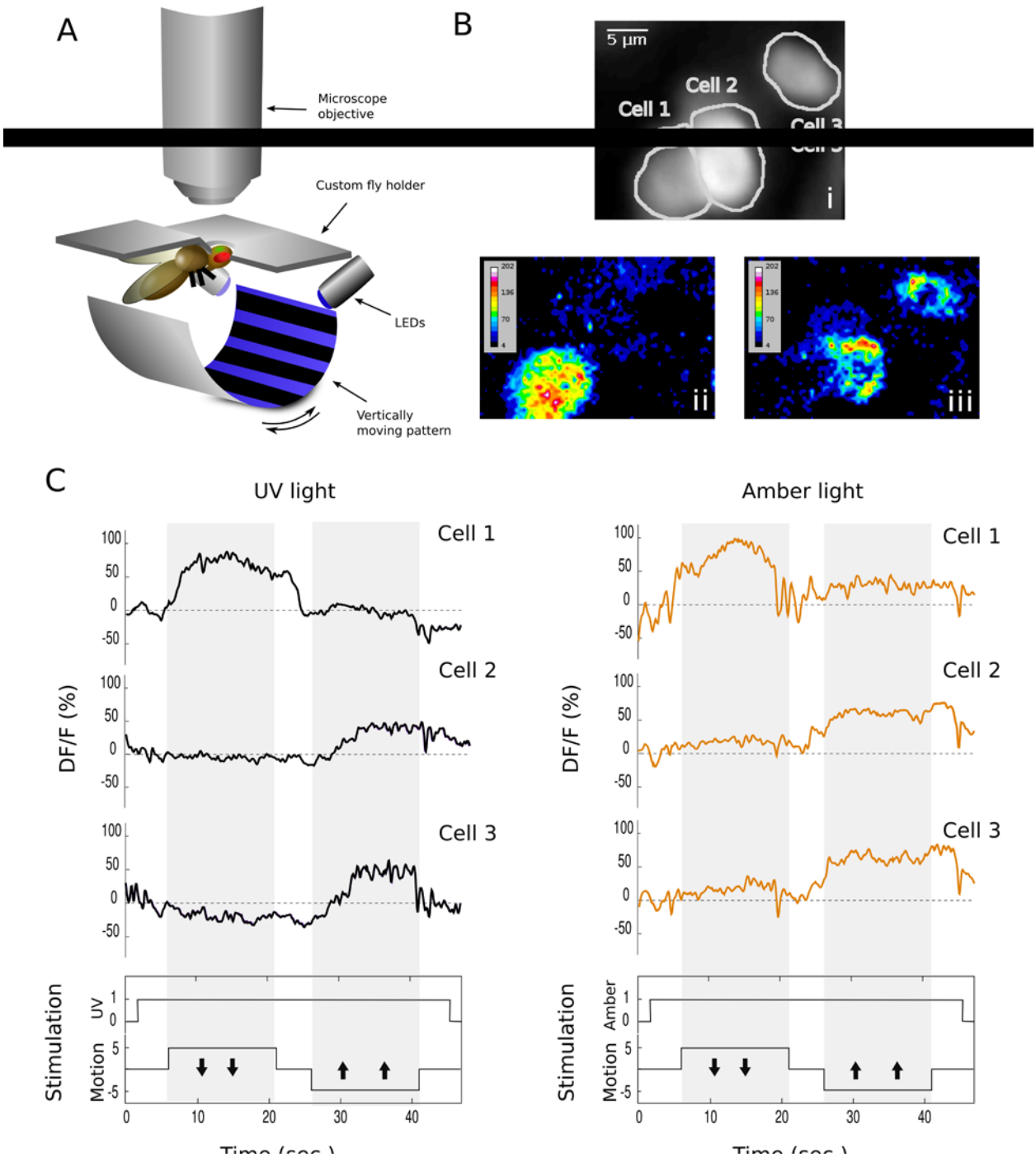

Fig. S12. Tangential cells in the lobula plate (LPTCs) of UV-flies respond selectively to top-down or bottom-up motion, similar to those of WT-flies (**fig. S14**), demonstrating normal motion-detection in their underlying circuits. (**A**) A customized 2-photon microscope system was used to visualize calcium-dependent fluorescence changes (from GCaMP3 optical reporter) in LPTCs to an up- or down-moving scene of different color. (**B**) Somatic fluorescence of three LPTCs was monitored simultaneously. Color-coded snapshots of their fluorescence output at 15 s and 35 s from the beginning of the experiment. (**C**) Their neural activity varied, with Cell1 responding to top-down (arrows down) UV (left) and amber (right) motion, as indicated by the relative increase in their fluorescence, while the two other cells responded to the corresponding bottom-up motion

(arrows up); these single recordings represent the largest responses to amber. See also **figs. S13-14.**

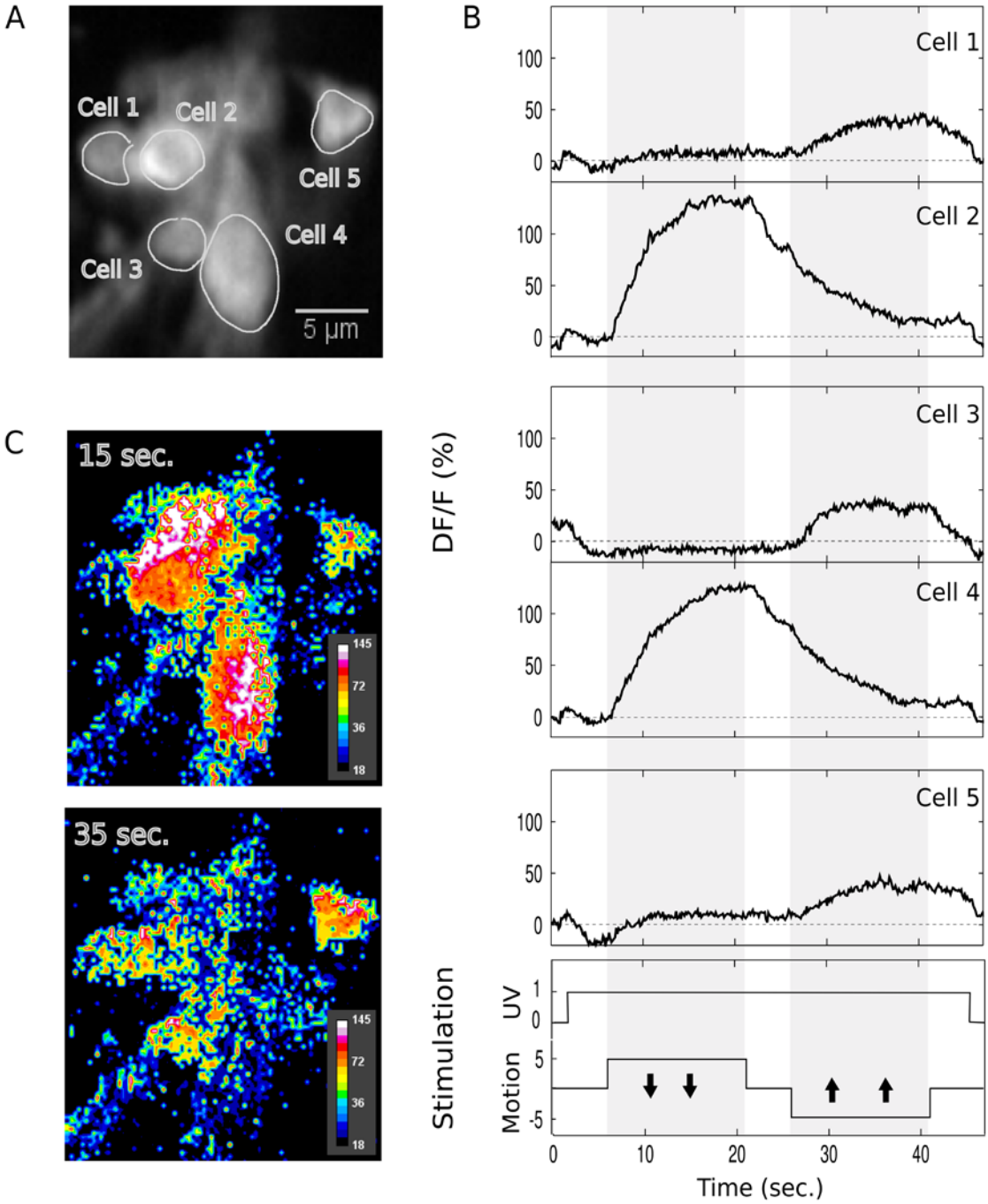

Fig. S13. In UV-flies during two-photon imaging, because of limited overlap between the infrared excitation of calcium-reporters and UV-sensitivity of R1-R6 photoreceptors, neural activity in multiple tangential cells (LPTCs; here Cell1-5) can be monitored simultaneously with high signal-to-noise ratio in the lobula plate. The tangential cells expressing GCaMP3.0 respond selectively to top-down or bottom-up motion UV-motion. (**A**) Their somatic fluorescence was monitored simultaneously. (**B**) Neural activity in LPTCs, as indicated by the relative increase in fluorescence (measured within the contoured areas in A), increased either during top-down (arrows down) or bottom-up motion (arrows up) UV motion. Interestingly, the neighbouring pairs (Cells 1 and 2; Cells 3 and 4; also Cells 1 and 2 in **fig. S12C**) generated opposing responses. (**C**) A color-

enhanced snapshots of their fluorescence output at 15 s and 35 s from the beginning of the experiment. Means of five consecutive experiments shown.

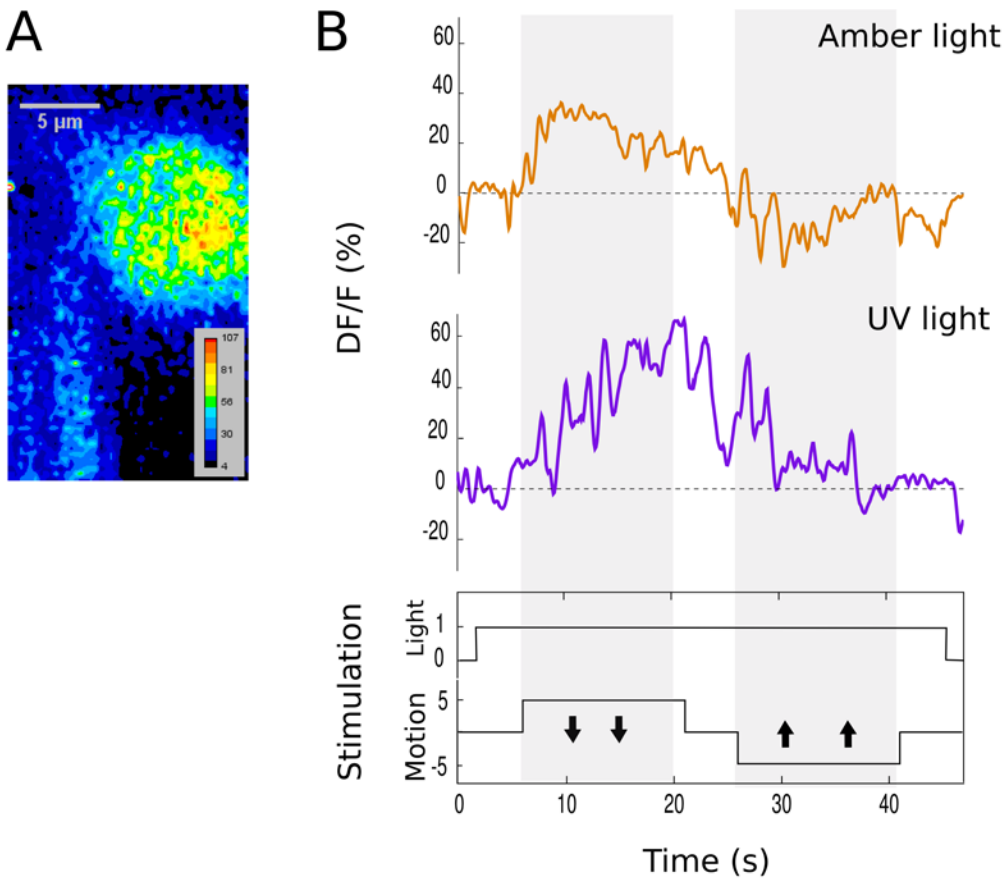

Fig. S14. An example of a lobula plate tangential cell of a fly, which expressed normal WT visual pigments in its photoreceptors, responded selectively to top-down motion of different colors, similar to that of UV-flies (**Fig. S12)**. (**A**) Its somatic fluorescence during top-down UV-motion; a color-enhanced snapshot taken at 15 s from the beginning of the experiment. (**B**) Its neural activity, as indicated by the relative increase in fluorescence, increased during top-down (arrows down) amber (above) and UV (below) motion. Consecutive single traces shown.

References

1. S. Nishida, J. Watanabe, I. Kuriki, T. Tokimoto, Human visual system integrates color signals along a motion trajectory. *Curr. Biol.* **17**, 366 (2007). doi:10.1016/j.cub.2006.12.041 Medline

2. T. Takeuchi, K. K. De Valois, J. L. Hardy, The influence of color on the perception of luminance motion. *Vision Res.* **43**, 1159 (2003). doi:10.1016/S0042-6989(03)00086-5 Medline

3. H. B. Barlow, The exploitation of regularities in the environment by the brain. *Behav. Brain Sci.* **24**, 602 (2001). doi:10.1017/S0140525X01000024 Medline

4. D. C. Knill, A. Pouget, The Bayesian brain: The role of uncertainty in neural coding and computation. *Trends Neurosci.* **27**, 712 (2004). doi:10.1016/j.tins.2004.10.007 Medline

5. P. H. Schiller, Parallel information processing channels created in the retina. *Proc. Natl. Acad. Sci. U.S.A.* **107**, 17087 (2010). doi:10.1073/pnas.1011782107 Medline

6. R. C. Hardie, Electrophysiological analysis of fly retina. I: Comparative properties of R1-6 and R 7 and 8. *J. Comp. Physiol. A* **129**, 19 (1979). doi:10.1007/BF00679908

7. S. J. Cropper, S. M. Wuerger, The perception of motion in chromatic stimuli. *Behav. Cogn. Neurosci. Rev.* **4**, 192 (2005). doi:10.1177/1534582305285120 Medline

8. K. R. Gegenfurtner, M. J. Hawken, Interaction of motion and color in the visual pathways. *Trends Neurosci.* **19**, 394 (1996). doi:10.1016/S0166-2236(96)10036-9 Medline

9. S. Yamaguchi, R. Wolf, C. Desplan, M. Heisenberg, Motion vision is independent of color in *Drosophila*. *Proc. Natl. Acad. Sci. U.S.A.* **105**, 4910 (2008). doi:10.1073/pnas.0711484105 Medline

10. A. M. Derrington, Vision: Can colour contribute to motion? *Curr. Biol.* **10**, R268 (2000). doi:10.1016/S0960-9822(00)00403-6 Medline

11. M. Joesch, B. Schnell, S. V. Raghu, D. F. Reiff, A. Borst, ON and OFF pathways in *Drosophila* motion vision. *Nature* **468**, 300 (2010). doi:10.1038/nature09545 Medline

12. M. Juusola, R. C. Hardie, Light adaptation in *Drosophila* photoreceptors: I. Response dynamics and signaling efficiency at 25 degrees C. *J. Gen. Physiol.* **117**, 3 (2001). doi:10.1085/jgp.117.1.3 Medline

13. L. Zheng *et al*., Feedback network controls photoreceptor output at the layer of first visual synapses in *Drosophila*. *J. Gen. Physiol.* **127**, 495 (2006). doi:10.1085/jgp.200509470 Medline

14. M. E. Chiappe, J. D. Seelig, M. B. Reiser, V. Jayaraman, Walking modulates speed sensitivity in *Drosophila* motion vision. *Curr. Biol.* **20**, 1470 (2010). doi:10.1016/j.cub.2010.06.072 Medline

15. S. G. Britt, R. Feiler, K. Kirschfeld, C. S. Zuker, Spectral tuning of rhodopsin and metarhodopsin in vivo. *Neuron* **11**, 29 (1993). doi:10.1016/0896-6273(93)90268-V Medline

16. W. H. Chou *et al*., Identification of a novel *Drosophila* opsin reveals specific patterning of the R7 and R8 photoreceptor cells. *Neuron* **17**, 1101 (1996). doi:10.1016/S0896-6273(00)80243-3 Medline

17. S. Gao *et al*., The neural substrate of spectral preference in *Drosophila*. *Neuron* **60**, 328 (2008). doi:10.1016/j.neuron.2008.08.010 Medline

18. J. Rister *et al*., Dissection of the peripheral motion channel in the visual system of *Drosophila melanogaster*. *Neuron* **56**, 155 (2007). doi:10.1016/j.neuron.2007.09.014 Medline

19. W. Kaiser, E. Liske, Die optomotorischen Reaktionen von fixiert fliegenden Bienen bei Reizung mit Spektrallichtern. *J. Comp. Physiol.* **89**, 391 (1974). doi:10.1007/BF00695355

20. M. Heisenberg, E. Buchner, The rôle of retinula cell types in visual behavior of *Drosophila melanogaster*. *J. Comp. Physiol.* **117**, 127 (1977). doi:10.1007/BF00612784

21. J. E. O'Tousa *et al*., The *Drosophila ninaE* gene encodes an opsin. *Cell* **40**, 839 (1985). doi:10.1016/0092-8674(85)90343-5 Medline

22. K. Kirschfeld, N. Franceschini, B. Minke, Evidence for a sensitising pigment in fly photoreceptors. *Nature* **269**, 386 (1977). doi:10.1038/269386a0 Medline

23. R. C. Hardie, A histamine-activated chloride channel involved in neurotransmission at a photoreceptor synapse. *Nature* **339**, 704 (1989). doi:10.1038/339704a0 Medline

24. S. Y. Takemura, Z. Lu, I. A. Meinertzhagen, Synaptic circuits of the *Drosophila* optic lobe: The input terminals to the medulla. *J. Comp. Neurol.* **509**, 493 (2008). doi:10.1002/cne.21757 Medline

25. B. Bausenwein, R. Wolf, M. Heisenberg, Genetic dissection of optomotor behavior in *Drosophila melanogaster*. Studies on wild-type and the mutant optomotor-blindH31. *J. Neurogenet.* **3**, 87 (1986). doi:10.3109/01677068609106897 Medline

26. G. G. de Polavieja, Neuronal algorithms that detect the temporal order of events. *Neural Comput.* **18**, 2102 (2006). doi:10.1162/neco.2006.18.9.2102 Medline

27. A. Riehle, N. Franceschini, Motion detection in flies: Parametric control over ON-OFF pathways. *Exp. Brain Res.* **54**, 390 (1984). doi:10.1007/BF00236243 Medline

28. S. R. Shaw, A. Fröhlich, I. A. Meinertzhagen, Direct connections between the R7/8 and R1-6 photoreceptor subsystems in the dipteran visual system. *Cell Tissue Res.* **257**, 295 (1989). doi:10.1007/BF00261833 Medline

29. S. R. Shaw, Early visual processing in insects. *J. Exp. Biol.* **112**, 225 (1984). Medline

30. I. A. Meinertzhagen, S. D. O'Neil, Synaptic organization of columnar elements in the lamina of the wild type in *Drosophila melanogaster*. *J. Comp. Neurol.* **305**, 232 (1991). doi:10.1002/cne.903050206 Medline

31. N. J. Scavarda, J. O'tousa, W. L. Pak, *Drosophila* locus with gene-dosage effects on rhodopsin. *Proc. Natl. Acad. Sci. U.S.A.* **80**, 4441 (1983). doi:10.1073/pnas.80.14.4441 Medline

32. R. Feiler *et al*., Ectopic expression of ultraviolet-rhodopsins in the blue photoreceptor cells of *Drosophila*: Visual physiology and photochemistry of transgenic animals. *J. Neurosci.* **12**, 3862 (1992). Medline

33. J. P. Kumar, D. F. Ready, Rhodopsin plays an essential structural role in *Drosophila* photoreceptor development. *Development* **121**, 4359 (1995). Medline

34. C. Gengs *et al*., The target of *Drosophila* photoreceptor synaptic transmission is a histamine-gated chloride channel encoded by ort (hclA). *J. Biol. Chem.* **277**, 42113 (2002). doi:10.1074/jbc.M207133200 Medline

35. C. H. Liu *et al*., Ca2+-dependent metarhodopsin inactivation mediated by calmodulin and NINAC myosin III. *Neuron* **59**, 778 (2008). doi:10.1016/j.neuron.2008.07.007 Medline

36. J. H. van Hateren, Electrical coupling of neuro-ommatidial photoreceptor cells in the blowfly. *J. Comp. Physiol. A* **158**, 795 (1986). doi:10.1007/BF01324822

37. M. Juusola, G. G. de Polavieja, The rate of information transfer of naturalistic stimulation by graded potentials. *J. Gen. Physiol.* **122**, 191 (2003). doi:10.1085/jgp.200308824 Medline

38. P. T. Gonzalez-Bellido, T. J. Wardill, M. Juusola, Compound eyes and retinal information processing in miniature dipteran species match their specific ecological demands. *Proc. Natl. Acad. Sci. U.S.A.* **108**, 4224 (2011). doi:10.1073/pnas.1014438108 Medline

39. D. A. Clark, L. Bursztyn, M. A. Horowitz, M. J. Schnitzer, T. R. Clandinin, Defining the computational structure of the motion detector in *Drosophila*. *Neuron* **70**, 1165 (2011). doi:10.1016/j.neuron.2011.05.023 Medline

40. H. Eichner, M. Joesch, B. Schnell, D. F. Reiff, A. Borst, Internal structure of the fly elementary motion detector. *Neuron* **70**, 1155 (2011). doi:10.1016/j.neuron.2011.03.028 Medline

41. M. V. Srinivasan, Shouldn't directional movement detection necessarily be "colour-blind"? *Vision Res.* **25**, 997 (1985). doi:10.1016/0042-6989(85)90210-X Medline

42. W. Kaiser, in *The Compound Eye and Vision of lnsects* (Clarendon, Oxford, 1975), pp. 359–377.

43. E. Salcedo *et al*., Blue- and green-absorbing visual pigments of *Drosophila*: Ectopic expression and physiological characterization of the R8 photoreceptor cell-specific Rh5 and Rh6 rhodopsins. *J. Neurosci.* **19**, 10716 (1999). Medline

44. L. Tian *et al*., Imaging neural activity in worms, flies and mice with improved GCaMP calcium indicators. *Nat. Methods* **6**, 875 (2009). doi:10.1038/nmeth.1398 Medline

45. E. K. Scott, T. Raabe, L. Luo, Structure of the vertical and horizontal system neurons of the lobula plate in *Drosophila*. *J. Comp. Neurol.* **454**, 470 (2002). doi:10.1002/cne.10467 Medline

46. P. T. Gonzalez-Bellido, T. J. Wardill, R. Kostyleva, I. A. Meinertzhagen, M. Juusola, Overexpressing temperature-sensitive dynamin decelerates phototransduction and bundles microtubules in *Drosophila* photoreceptors. *J. Neurosci.* **29**, 14199 (2009). doi:10.1523/JNEUROSCI.2873-09.2009 Medline

47. S. T. Ahmad, M. Natochin, N. O. Artemyev, J. E. O'Tousa, The *Drosophila* rhodopsin cytoplasmic tail domain is required for maintenance of rhabdomere structure. *FASEB J.* **21**, 449 (2007). doi:10.1096/fj.06-6530com Medline

48. S. V. Raghu, M. Joesch, A. Borst, D. F. Reiff, Synaptic organization of lobula plate tangential cells in *Drosophila*: gamma-aminobutyric acid receptors and chemical release sites. *J. Comp. Neurol.* **502**, 598 (2007). doi:10.1002/cne.21319 Medline

49. M. Mank *et al*., A genetically encoded calcium indicator for chronic in vivo two-photon imaging. *Nat. Methods* **5**, 805 (2008). doi:10.1038/nmeth.1243 Medline

50. Y. Zhu, A. Nern, S. L. Zipursky, M. A. Frye, Peripheral visual circuits functionally segregate motion and phototaxis behaviors in the fly. *Curr. Biol.* **19**, 613 (2009). doi:10.1016/j.cub.2009.02.053 Medline

51. R. C. Hardie, INDO-1 measurements of absolute resting and light-induced Ca2+ concentration in *Drosophila* photoreceptors. *J. Neurosci.* **16**, 2924 (1996). Medline

52. R. C. Hardie, F. Martin, S. Chyb, P. Raghu, Rescue of light responses in the *Drosophila* "null" phospholipase C mutant, norpAP24, by the diacylglycerol kinase mutant, rdgA, and by metabolic inhibition. *J. Biol. Chem.* **278**, 18851 (2003). doi:10.1074/jbc.M300310200 Medline

53. M. T. Pearn, L. L. Randall, R. D. Shortridge, M. G. Burg, W. L. Pak, Molecular, biochemical, and electrophysiological characterization of *Drosophila* norpA mutants. *J. Biol. Chem.* **271**, 4937 (1996). doi:10.1074/jbc.271.9.4937 Medline

54. T. Washburn, J. E. O'Tousa, Molecular defects in *Drosophila* rhodopsin mutants. *J. Biol. Chem.* **264**, 15464 (1989). Medline

55. H. Luan, N. C. Peabody, C. R. Vinson, B. H. White, Refined spatial manipulation of neuronal function by combinatorial restriction of transgene expression. *Neuron* **52**, 425 (2006). doi:10.1016/j.neuron.2006.08.028 Medline

56. M. Juusola, R. C. Hardie, *J. Gen. Physiol.* **117**, 191 (2001).

57. I. A. Meinertzhagen, Ultrastructure and quantification of synapses in the insect nervous system. *J. Neurosci. Methods* **69**, 59 (1996). doi:10.1016/S0165-0270(96)00021-0 Medline

58. L. Zheng *et al*., Network adaptation improves temporal representation of naturalistic stimuli in *Drosophila* eye: I dynamics. *PLoS ONE* **4**, e4307 (2009). doi:10.1371/journal.pone.0004307 Medline

59. M. Juusola, M. Weckström, Band-pass filtering by voltage-dependent membrane in an insect photoreceptor. *Neurosci. Lett.* **154**, 84 (1993). doi:10.1016/0304-3940(93)90177-M Medline

60. M. Weckström, E. Kouvalainen, M. Juusola, Measurement of cell impedance in frequency domain using discontinuous current clamp and white-noise-modulated current injection. *Pflugers Arch.* **421**, 469 (1992). doi:10.1007/BF00370258 Medline

61. J. H. van Hateren, Processing of natural time series of intensities by the visual system of the blowfly. *Vision Res.* **37**, 3407 (1997). doi:10.1016/S0042-6989(97)00105-3 Medline

62. M. Juusola, R. O. Uusitalo, M. Weckström, Transfer of graded potentials at the photoreceptor-interneuron synapse. *J. Gen. Physiol.* **105**, 117 (1995). doi:10.1085/jgp.105.1.117 Medline

63. R. O. Uusitalo, M. Juusola, M. Weckström, Graded responses and spiking properties of identified first-order visual interneurons of the fly compound eye. *J. Neurophysiol.* **73**, 1782 (1995). Medline

64. K.-F. Fischbach, A. P. M. Dittrich, The optic lobe of *Drosophila melanogaster*. I. A Golgi analysis of wild-type structure. *Cell Tissue Res.* **258**, 441 (1989). doi:10.1007/BF00218858

65. A. Kolodziejczyk, X. Sun, I. A. Meinertzhagen, D. R. Nässel, Glutamate, GABA and acetylcholine signaling components in the lamina of the *Drosophila* visual system. *PLoS ONE* **3**, e2110 (2008). doi:10.1371/journal.pone.0002110 Medline

66. M. Vähäsöyrinki, J. E. Niven, R. C. Hardie, M. Weckström, M. Juusola, Robustness of neural coding in *Drosophila* photoreceptors in the absence of slow delayed rectifier K+ channels. *J. Neurosci.* **26**, 2652 (2006). doi:10.1523/JNEUROSCI.3316-05.2006 Medline

67. M. Juusola, E. Kouvalainen, M. Järvilehto, M. Weckström, Contrast gain, signal-to-noise ratio, and linearity in light-adapted blowfly photoreceptors. *J. Gen. Physiol.* **104**, 593 (1994). doi:10.1085/jgp.104.3.593 Medline

68. C. E. Shannon, *Bell Syst. Tech. J.* **27**, 379 (1948).

69. R. C. Hardie *et al*., Molecular basis of amplification in *Drosophila* phototransduction: Roles for G protein, phospholipase C, and diacylglycerol kinase. *Neuron* **36**, 689 (2002). doi:10.1016/S0896-6273(02)01048-6 Medline

70. V. I. Govardovskii, N. Fyhrquist, T. Reuter, D. G. Kuzmin, K. Donner, In search of the visual pigment template. *Vis. Neurosci.* **17**, 509 (2000). doi:10.1017/S0952523800174036 Medline

71. R. C. Hardie, K. Kirschfeld, Ultraviolet sensitivity of fly photoreceptors R7 and R8: Evidence for a sensitising function. *Biophys. Struct. Mech.* **9**, 171 (1983). doi:10.1007/BF00537814

72. K. I. Naka, W. A. H. Rushton, *J. Physiol. (London)* **185**, 587 (1966).

73. S. Tang, A. Guo, Choice behavior of *Drosophila* facing contradictory visual cues. *Science* **294**, 1543 (2001). doi:10.1126/science.1058237 Medline

74. S. Tang, R. Wolf, S. Xu, M. Heisenberg, Visual pattern recognition in *Drosophila* is invariant for retinal position. *Science* **305**, 1020 (2004). doi:10.1126/science.1099839 Medline

75. K. G. Götz, [Optomoter studies of the visual system of several eye mutants of the fruit fly *Drosophila*]. *Kybernetik* **2**, 77 (1964). Medline

76. M. Heisenberg, R. Wolf, *Vision in* Drosophila: *Genetics of Microbehavior*, vol. 12 of *Studies of Brain Function* (Springer Verlag, Berlin, 1985).

77. A. Hopt, E. Neher, Highly nonlinear photodamage in two-photon fluorescence microscopy. *Biophys. J.* **80**, 2029 (2001). doi:10.1016/S0006-3495(01)76173-5 Medline

78. J. D. Seelig *et al*., Two-photon calcium imaging from head-fixed Drosophila during optomotor walking behavior. *Nat. Methods* **7**, 535 (2010). doi:10.1038/nmeth.1468 Medline

79. M. Rivera-Alba *et al*., Wiring economy and volume exclusion determine neuronal placement in the *Drosophila* brain. *Curr. Biol.* **21**, 2000 (2011). doi:10.1016/j.cub.2011.10.022 Medline

80. I. Sinakevitch, N. J. Strausfeld, Chemical neuroanatomy of the fly's movement detection pathway. *J. Comp. Neurol.* **468**, 6 (2004). doi:10.1002/cne.10929 Medline

81. S. Y. Takemura *et al*., Cholinergic circuits integrate neighboring visual signals in a *Drosophila* motion detection pathway. *Curr. Biol.* **21**, 2077 (2011). doi:10.1016/j.cub.2011.10.053 Medline

82. A. Nikolaev *et al*., Network adaptation improves temporal representation of naturalistic stimuli in *Drosophila* eye: II mechanisms. *PLoS ONE* **4**, e4306 (2009). doi:10.1371/journal.pone.0004306 Medline

83. M. Weckstrom, M. Juusola, S. B. Laughlin, Presynaptic Enhancement of Signal Transients in Photoreceptor Terminals in the Compound Eye. *Proc. R. Soc. London Ser. B* **250**, 83 (1992). doi:10.1098/rspb.1992.0134

84. J. H. van Hateren, S. B. Laughlin, *J. Comp. Physiol. A* **166**, 437 (1990).

85. J. M. Karpilow, A. C. Pimentel, H. K. Shamloula, T. R. Venkatesh, Neuronal development in the *Drosophila* compound eye: Photoreceptor cells R1, R6, and R7 fail to differentiate in the retina aberrant in pattern (rap) mutant. *J. Neurobiol.* **31**, 149 (1996). doi:10.1002/(SICI)1097-4695(199610)31:2<149::AID-NEU2>3.0.CO;2-B Medline

86. R. Strauss, M. Renner, K. Gotz, Task-specific association of photoreceptor systems and steering parameters in *Drosophila*. *J. Comp. Physiol. A* **187**, 617 (2001). doi:10.1007/s003590100234

87. P. R. Hiesinger *et al*., Activity-independent prespecification of synaptic partners in the visual map of *Drosophila*. *Curr. Biol.* **16**, 1835 (2006). doi:10.1016/j.cub.2006.07.047 Medline

88. T. Wang, U. Lao, B. A. Edgar, TOR-mediated autophagy regulates cell death in *Drosophila* neurodegenerative disease. *J. Cell Biol.* **186**, 703 (2009). doi:10.1083/jcb.200904090 Medline

89. T. Kitamoto, Conditional modification of behavior in *Drosophila* by targeted expression of a temperature-sensitive shibire allele in defined neurons. *J. Neurobiol.* **47**, 81 (2001). doi:10.1002/neu.1018 Medline

90. S. T. Hong *et al*., Histamine and its receptors modulate temperature-preference behaviors in *Drosophila*. *J. Neurosci.* **26**, 7245 (2006). doi:10.1523/JNEUROSCI.5426-05.2006 Medline

91. M. Freeman, Reiterative use of the EGF receptor triggers differentiation of all cell types in the *Drosophila* eye. *Cell* **87**, 651 (1996). doi:10.1016/S0092-8674(00)81385-9 Medline

92. J. M. Kramer, B. E. Staveley, GAL4 causes developmental defects and apoptosis when expressed in the developing eye of *Drosophila melanogaster*. *Genet. Mol. Res.* **2**, 43 (2003). Medline

93. A. Keller, S. T. Sweeney, T. Zars, C. J. O'Kane, M. Heisenberg, Targeted expression of tetanus neurotoxin interferes with behavioral responses to sensory input in *Drosophila*. *J. Neurobiol.* **50**, 221 (2002). doi:10.1002/neu.10029 Medline

94. D. Hadjieconomou *et al*., Flybow: Genetic multicolor cell labeling for neural circuit analysis in *Drosophila melanogaster*. *Nat. Methods* **8**, 260 (2011) (Mar). doi:10.1038/nmeth.1567 Medline

95. S. C. Hoyer *et al*., Octopamine in male aggression of *Drosophila*. *Curr. Biol.* **18**, 159 (2008). doi:10.1016/j.cub.2007.12.052 Medline

96. S. G. Sprecher, C. Desplan, Switch of rhodopsin expression in terminally differentiated *Drosophila* sensory neurons. *Nature* **454**, 533 (2008). doi:10.1038/nature07062 Medline

97. T. Cook, F. Pichaud, R. Sonneville, D. Papatsenko, C. Desplan, Distinction between color photoreceptor cell fates is controlled by Prospero in *Drosophila*. *Dev. Cell* **4**, 853 (2003). doi:10.1016/S1534-5807(03)00156-4 Medline

98. A. Huber *et al*., Molecular cloning of *Drosophila* Rh6 rhodopsin: The visual pigment of a subset of R8 photoreceptor cells. *FEBS Lett.* **406**, 6 (1997). doi:10.1016/S0014-5793(97)00210-X Medline

99. A. G. Reaume, D. A. Knecht, A. Chovnick, The rosy locus in *Drosophila melanogaster*: Xanthine dehydrogenase and eye pigments. *Genetics* **129**, 1099 (1991). Medline

100. S. Wicks, N. Bain, A. Duttaroy, A. J. Hilliker, J. P. Phillips, Hypoxia rescues early mortality conferred by superoxide dismutase deficiency. *Free Radic. Biol. Med.* **46**, 176 (2009). doi:10.1016/j.freeradbiomed.2008.09.036 Medline

101. L. M. Newby, F. R. Jackson, *Drosophila* ebony mutants have altered circadian activity rhythms but normal eclosion rhythms. *J. Neurogenet.* **7**, 85 (1991). doi:10.3109/01677069109066213 Medline

102. J. Borycz, J. A. Borycz, M. Loubani, I. A. Meinertzhagen, tan and ebony genes regulate a novel pathway for transmitter metabolism at fly photoreceptor terminals. *J. Neurosci.* **22**, 10549 (2002). Medline

103. A. M. Phillips, R. Smart, R. Strauss, B. Brembs, L. E. Kelly, The *Drosophila* black enigma: The molecular and behavioural characterization of the black1 mutant allele. *Gene* **351**, 131 (2005). doi:10.1016/j.gene.2005.03.013 Medline

104. J. E. Niven *et al*., The contribution of Shaker K+ channels to the information capacity of *Drosophila* photoreceptors. *Nature* **421**, 630 (2003). doi:10.1038/nature01384 Medline

105. R. C. Hardie, Voltage-sensitive potassium channels in *Drosophila* photoreceptors. *J. Neurosci.* **11**, 3079 (1991). Medline